In: Soft Condensed Matter: New Research
Editor: Kathy I. Dillon, pp. 291-335
ISBN 1-59454-665-7

Chapter 10

DYNAMICS OF SEMIRIGID ROD POLYMERS FROM EXPERIMENTAL STUDIES

George D. J. Phillies[1] ***and Kiril A. Streletzky***[2]
[1]Department of Physics, Worcester Polytechnic Institute,
Worcester, Massachusetts
[2]Department of Physics, Cleveland State University,
Cleveland, Ohio

Abstract

Experimental measurements of static and dynamic properties of non-ionic polymer solutions provide good testing grounds for existing and new models of polymer solution dynamics. We extensively studied aqueous solutions of the high molecular weight, rodlike, semiflexible polymer hydroxypropylcellulose (HPC). Here we present our systematic analysis of measurements of: a) low-shear viscosity η, b) quasi-elastic light scattering spectra of HPC solutions, including mode structure analysis at a range of temperatures and concentrations, c) quasi-elastic light scattering spectra of optical probe particles diffusing through HPC solutions, including careful characterization of modes of diffusive relaxation for tracer particles of different sizes, and d) static light scattering.

We found a variety of novel phenomena. (i) The functional dependence of η on concentration has a transition at c^+, with disparate small- and large- concentration dependences being seen. For $c < c^+$, η depends on c via a stretched exponential $\exp(-ac^\nu)$ in c ("solution-like" behavior). For $c > c^+$, η depends on c via a power law $\eta \sim c^x$ with $x \approx 4$ ("meltlike" behavior). The viscometric crossover at c^+ is echoed by the probe diffusion data, confirming the physical reality of the solution-to-meltlike transition. (ii) Optical probe spectra and polymer spectra are both strongly non-exponential and can be decomposed into two or (at larger polymer concentrations) three spectral modes. Mode structure analysis reveals that probe relaxations and polymer relaxations in the same solution sample different aspects of polymer dynamics. (iii) Except for the largest (0.76μm) probes, diffusion coefficients of tracer particles in polymer solutions are not determined by the solution macroscopic viscosity. (iv) At concentrations above c^+, light scattering spectra of HPC in solution have an ultraslow relaxational mode. This mode exhibits properties expected for long-lived dynamic structures but not the properties expected for local equilibrium regions of elevated polymer concentration. Properties of the slow mode are consistent with predictions from some models of glass formation. Finally, (v) polymer solutions have a

characteristic dynamic length, which is approximately the hydrodynamic radius of the polymer.

1 Introduction

The nature of polymer dynamics *in solution* remains a matter of study. A family of models[1, 2], based on the dominant importance of chain crossing constraints as dynamic transient restraints on lateral chain motions, is widely believed to have captured many important features of polymer dynamics in the polymer *melt* phase. These models have been used to describe diffusion of individual polymer molecules, whole-chain and segment diffusion, linear viscoelastic behavior, dielectric response, and the effect of chain branching in polymer melts. Challenges to these models remain, involving such questions as fluctuations around average chain behavior, the size of the transient entanglement tube and its shape under deformation, and nonlinear viscoelastic behavior[2].

In solution, matters are more complex. In solution, a variety of forces compete to determine how polymers move. Competing forces include short-range excluded-volume interactions, longer range forces such as the van der Waals interaction, chain crossing (topological) constraints, and the long-range solvent-mediated hydrodynamic interaction. The relative importance of these forces is assigned differently by different authors. Some authors propose that chain crossing constraints are dominant, leading to the validity of tube- or reptation-based descriptions of polymer motions, by analogy with seemingly valid models for polymer melts[3]. Other authors assert the primacy of hydrodynamic forces[4].

For solutions, reviews [5, 6, 7, 8] find "...an abundance of evidence exists that argues against the simple reptation model's validity"[6], "The results on the concentration dependence of [the polymer self-diffusion coefficient] in polymer solutions are also not in accord with the prediction based on the reptation model"[7], or "it is unlikely that reptation is significant in the semidilute regime,..."[8]. Whatever may be the circumstance for melts, the nature of polymer dynamics for polymers in solution remains a topic of inquiry.

Due to the easy experimental accessibility of its lyotropic phase, hydroxypropylcellulose (HPC) solutions have become an important testing ground in several domains of macromolecular science. Reversible phase separation and the formation of liquid-crystalline domains in HPC solutions make this system interesting for phase transition studies[9, 10, 11]. The intriguing rheological behavior and molecular orientation of the HPC liquid crystalline system under shear flow has also been examined[12, 13, 14]. Aqueous solutions of HPC are surface active; thin films obtained from isotropic polymer solutions have been widely studied[15] and used as an alignment substrate in liquid-crystal electro-optical devices[16]. Temperature driven macromolecular association of HPC in solution, due to a dissolved high gain laser dye, can be used to tune the intensity and wavelength of random lasing systems[17]. Temperature-tunable random laser systems can be useful microscale temperature sensors, or pixel scale heating elements in optical displays[17].

Common applications of HPC include being an FDA-approved non-toxic food additive, found in soups and ice creams as an emulsifier[18] and encapsulator[19]. There are also many pharmaceutical applications of HPC. The most exciting of these arise from the amphiphilic nature of HPC molecules. The co-presence of hydrophobic and hydrophilic regions in HPC molecules allows numerous designs for a controlled drug release mecha-

nism, both in solution and from gel forms. First, in the presence of hydrophobic agents, HPC in solution can form polymeric micelles, which are a highly effective drug delivery system[20]. Second, by changing the properties of the solvent, one can induce polymer self-association into hydrogel nanoparticles which can be used for controlled drug delivery[21]. Third, an HPC matrix in a dissolving medium can swell or deswell, depending on polymer hydration, acting as a thermally-reversible hydrogel medium[22]. The hydrogel is a temperature-sensitive drug delivery medium that extracts water and small solutes from aqueous solution when it expands, and releases them when it collapses[22].

As part of a systematic examination of the nature of polymer dynamics, this laboratory has performed extensive experimental studies on the viscosity and relaxational modes of aqueous HPC solutions [23, 24, 25, 26, 27, 28, 29, 30, 31]. As described below, we have examined viscosity, static light scattering, quasi-elastic light scattering spectra of the polymer itself, and quasi-elastic light scattering spectra of optical probe particles diffusing through HPC solutions. These measurements are supplemented by measurements from elsewhere on the diffusion of dye molecules[32] and labelled dextrans[33] through the same solutions. Comparisons can then be made with reptation and hydrodynamic scaling models for polymer dynamics[3], with coupling models for interacting objects[34, 35, 36, 37, 38, 39], and with modern theories of the glass transition[40].

Hydroxypropylcellulose(HPC) is a chemically-modified water-soluble polysaccharide. The polymer chain is relatively stiff, with a persistence length of approximately 10 nm[41, 42, 43]. The solvation of HPC is temperature-dependent. At 10C, water is a good solvent for HPC. At approximately 40C, water becomes a pseudotheta solvent for HPC, so that with increasing temperature solutions become first lucent and then opaque[32]. HPC: water mixtures have a lyotropic phase transition. At 25 C, the transition begins in the concentration range 360-420 g/L[10].

HPC is of particular interest experimentally because it is somewhat rigid, is soluble in a wide range of solvents, and unlike many somewhat rigid polymers is electrically neutral. The last feature has the positive outcome that HPC solutions support study of solution dynamics of semirigid rods without suffering from complications attendant to polyelectrolyte phenomena. The dynamics of HPC molecules in solution have been studied with a wide range of physical techniques, including as discussed below low-shear viscometry, frequency-dependent rheometry, static and quasielastic light scattering, and optical probe diffusion.

Over the past decade, this laboratory has made systematic studies of dynamic properties of hydroxypropylcellulose: water solution using modern physical techniques. When united as seen here, and coupled with parallel studies in other laboratories, our studies lead to a coherent picture of relaxational modes, fundamental length scales, and the physical nature of observed dynamic transitions in HPC solutions. This picture, as seen below, has deep resonances with certain modern theories of the liquid pre-glass transition.

The next Section of this Chapter treats experimental methodologies, including physical means of mutual and self diffusion processes and probe diffusion, relationships between probe spectra and particle motions, and spectral fitting functions and parameters for interpreting our multimodal light scattering spectra. Section Three presents a phenomenological description of the dynamics of aqueous hydroxypropylcellulose, including the solution viscosity, static light scattering, quasi-elastic light scattering spectra of HPC: water, and optical

probe measurements of HPC:water solutions. Section Four compares our results with the Ngai-Rendell coupling model. Section Five reports Conclusions.

2 Experimental Methods

Much past experimental work in this laboratory employed quasi-elastic light scattering spectroscopy (QELSS) and, more recently, static light scattering to study equilibrium solution samples illuminated by a laser beam. Static light scattering determines the average intensity of the laser light scattered into a given direction. Quasielastic light scattering spectroscopy statistically characterizes the temporal evolution of fluctuations in the intensity of the scattered light. Under exactly the right conditions, the fluctuations are in a time and brightness range that the naked eye can see: With appropriate safety precautions, the scattered light is seen to twinkle when projected onto a flat screen.

In either experimental technique, an equilibriated polymer solution is illuminated by a pencil of monochromatic, coherent light, in this laboratory from an argon-ion laser or a diode-pumped solid-state laser. Light is scattered by each polymer subunit and by other objects in solution. Because the light is coherent, light scattered by different subunits interferes, constructively or destructively. When the objects in solution move, the degree of interference changes. Correspondingly, the intensity of the light scattered through a given angle into a given direction fluctuates in time.

Polymer motion in solution is diffusive. Polymer chains perform Brownian motion, generally with strong interactions between Brownian units. Brownian motion that takes place over the distance scale to which QELSS is sensitive imbues QELSS spectra with relaxations on the time scales on which the chains move over the distance scale. Statistical properties of the particle motion are mirrored by statistical properties of the temporal evolution of the scattering intensity, so inferences about solution dynamics can be made from light scattering. Each spectral relaxation corresponds to a diffusion coefficient or, in more complex systems, to a diffusive process of the polymers in solution.

2.1 Diffusion Processes

We usefully distinguish between three independent diffusion coefficients in HPC solutions. Two coefficients refer to polymer:solvent mixtures. The third diffusion coefficient refers to ternary polymer:solvent:tracer systems. If the solution only contains the solvent and HPC molecules: The self- or tracer-diffusion coefficient D_s characterizes the motion of a single HPC molecule through the solution. The mutual diffusion coefficient D_m characterizes the relaxation of a polymer concentration gradient. In terms of Fick's law of diffusion

$$\vec{J}(\mathbf{r},t) = D_m \vec{\nabla} c(\mathbf{r},t), \tag{1}$$

D_m links the diffusion current $\vec{J}$ and the macromolecule concentration c at position and time $(\mathbf{r},t)$. If intermacromolecular interactions have an extended range, $\vec{J}(\mathbf{r},t)$ will depend on c over a region centered on $\mathbf{r}$ and t. D_m may properly be said to characterize the relative diffusive motion of pairs of molecules. In a monodisperse system, quasi-elastic light scattering spectroscopy (QELSS) determines D_m [44, 45]. The self-diffusion coefficient can be measured with pulsed-field-gradient nuclear magnetic resonance (PFGNMR).

A third diffusion coefficient is experimentally accessible by studying a ternary system that contains solvent and two distinct macrocomponents. Such systems have at least two relaxation times, each describing a coupled mode involving the concentrations of both macromolecules. It is particularly interesting to study the special case in which one macromolecule species–the *probe*–is dilute; the other macromolecule species–the *matrix*–may have any concentration. In this special case, diffusion of the probe species is governed by a single-particle diffusion coefficient, namely the probe diffusion coefficient D_p.

Several distinct measurements can be described as determining probe diffusion:

First, the probe molecules might be matrix molecules to which a small dye fragment or other label has been attached. Measurements on the labelled macromolecules with Fluorescence Recovery After Photobleaching (FRAP) or Forced Rayleigh Scattering (FRS) determine D_p. If the dye fragment is much smaller than the labelled macromolecule, D_p is not distinguishable from the self-diffusion coefficient D_s of the matrix.

Second, the probe and matrix species might be unlike polymers, differing in their molecular weights or perhaps even their species. By studying homologous probes and matrices, the experimenter can disentangle how D_s is affected by the molecular weight of the moving molecule of interest and, separately, by the molecular weight and concentration of the matrix molecules that surround the molecule of interest.

Third, the probes might be very different from the matrix species. In the cases here, the matrix species is HPC, while the probes are polystyrene latex spheres or dextrans[33]. If the matrix species and solvent are nearly isorefractive, the matrix scatters almost no light. The intensely-scattering polystyrene spheres then dominate the QELSS spectrum. In this special case, the diffusion coefficient measured by QELSS is[45, 46] the probe diffusion coefficient D_p. Microsphere diffusion in polymer solutions has been studied intensely for almost three decades[47].

Experimental methods are sensitive to molecular motions over a range of time and distance scales. Instead of saying that one measures a diffusion *coefficient*, it is more precise to say one measures a diffusion *process*. Diffusion processes, which may be characterized by several time scales or relaxation lengths, correspond to the microscopic molecular motions to which each experimental method is sensitive.

2.2 QELSS and Macroparticle Motion

How is a QELSS measurement related to particle motions? The observed light scattering spectrum $S(q,\tau)$, which is the intensity-intensity autocorrelation function of the incident laser light scattered by the sample into a particular direction, is linked to the microscopic system[48] via the field correlation function $g^{(1)}(q,\tau)$, namely

$$S(q,\tau) = A(g^{(1)}(q,\tau))^2 + B. \tag{2}$$

In this equation, A and B are constants determined by the photocount rate, integration time, coherency across the photomultiplier tube front surface, amount of stray light, and other apparatus-dependent factors. $\mathbf{q}$ is the scattering vector; its magnitude is q. τ is the delay time.

The field correlation function $g^{(1)}(q,\tau)$ is in turn determined by the positions and motions of the scattering molecules, namely

$$g^{(1)}(q,\tau) = \left\langle \sum_{i,j=1}^{N} \alpha_i \alpha_j \exp[i\mathbf{q}\cdot(\mathbf{r}_i(t+\tau) - \mathbf{r}_j(t))] \right\rangle. \tag{3}$$

Here i and j label a pair of the N scatterers. $\mathbf{r}_j(t)$ is the position of scatterer j at time t. α_i^2 is the scattering cross-section of particle i. If polymer chains are substantially smaller than a light wavelength, each chain is effectively a single scattering particle. With larger chains, interference between scattering from different parts of a chain becomes important, and i and j usefully refer to segments of larger polymer chains. In two-component macromolecule:solvent solutions, QELSS measures the correlation between a displacement (namely the displacement $\mathbf{r}_i(t+\tau) - \mathbf{r}_i(t)$ of a scatterer i, between times t and $t+\tau$) and an initial relative position (namely the relative position $\mathbf{r}_i(t) - \mathbf{r}_j(t)$ of scatterers i and j, at time t). Note that i and j are allowed to refer to the same scatterer.

In a three-component solution in which one macromolecule species scatters no light, and in which the scattering component is dilute, correlations between the positions of different scatterers vanish. The field correlation function then assumes its *probe* form

$$g_P^{(1)}(q,\tau) = \left\langle \sum_{i=1}^{N} \alpha_i^2 \exp[i\mathbf{q}\cdot\Delta\mathbf{r}_i(\tau)] \right\rangle. \tag{4}$$

Here we introduce the notation $\Delta\mathbf{r}_i(\tau) = \mathbf{r}_i(t+\tau) - \mathbf{r}_i(t))$.

If the scattering particles are performing orthodox Brownian motion, as is the case for highly dilute probe particles in a simple Newtonian (non-viscoelastic) solvent, $g_P^{(1)}(q,\tau)$ can be simplified further. This simplification describes, e.g., dilute polystyrene spheres diffusing in room temperature water. This simplification does not describe the diffusion of probe spheres in a viscoelastic or structured medium such as a polymer solution. The simplification begins with Berne and Pecora [48], who present a treatment of the scattering spectrum for dilute, noninteracting *Brownian* particles. The probability distribution for the displacements $\Delta\mathbf{R}$ of an isolated Brownian particle, whose motion follows the Langevin equation, is given by the Central Limit Theorem as

$$G_s(\Delta\mathbf{R},\tau) = \left[\frac{2\pi}{3}\langle(\Delta\mathbf{R})^2\rangle\right]^{-3/2} \exp\left[-3(\Delta R)^2/2\langle(\Delta\mathbf{R})^2\rangle\right], \tag{5}$$

where τ is the time over which the displacements $\delta\mathbf{R}$ are to occur. In this equation, the mean-square particle displacement is

$$\langle(\Delta\mathbf{R})^2\rangle = 6D\tau, \tag{6}$$

D being the single-particle diffusion coefficient. Eqs 4, 5, and 6 give

$$g_P^{(1)}(q,\tau) \sim \exp(-q^2 D\tau). \tag{7}$$

For dilute Brownian spheres in small-molecule low-viscosity solvents, the Stokes-Einstein equation

$$D = \frac{k_B T}{6\pi\eta R} \tag{8}$$

is reasonably accurate. Here k_B, η, R, and T are Boltzmann's constant, the solvent viscosity, the sphere radius, and the absolute temperature. If the solution is sufficiently concentrated that the solvent viscosity and solution viscosity differ appreciably, eq 8 is not applicable. As first noted by Altenberger and Deutch[49], Brownian particles have a long-range ($1/r$ force) hydrodynamic interaction described to first approximation by the Oseen tensor, so the approximation that dilute Brownian particles are non-interacting is fundamentally incorrect. However, as shown by Altenberger and Deutch, when the Oseen interaction is correctly included in a calculation of $g^{(1)}(q,\tau)$, the corrections to the non-interacting expression vanish at low particle concentration.

The experiments described below refer to dilute Brownian particles diffusing through complex fluids having multiple length and time scales. These experiments refer to systems in which the simple Brownian particle picture is entirely inappropriate. To render the Brownian particle picture applicable to probe motion in polymer solutions, two *ad hoc* extensions have been employed:

First, in some systems the Brownian particles appear to be performing orthodox diffusion, but D does not agree with the Stokes-Einstein equation, no matter whether η is taken to be the solvent viscosity or the solution viscosity. In this case, the Stokes-Einstein equation is sometimes taken to *define* a microviscosity η_μ via

$$\eta_\mu = \frac{k_B T}{6\pi D R}. \tag{9}$$

η_μ may be compared with the solvent and solution viscosities obtained with classical instruments, as seen below.

Second, it is sometimes proposed that the form

$$g^{(1)}(q,\tau) \equiv \langle \exp[i\mathbf{q}\cdot\blacksquare\mathbf{r}]\rangle = \exp\left[-q^2\left\langle(\Delta\mathbf{r})^2\right\rangle/6\right] \tag{10}$$

is uniformly applicable to light scattering spectra. Eq 10 asserts that the average of the exponential is the exponential of a particular average. This assertion would be correct if $\Delta\mathbf{r}$ were governed by a Gaussian-random Markoff process. Brownian particles whose motions are governed by the Langevin equation do indeed have successive displacements described by Gaussian-random Markoff processes. However, if $\Delta\mathbf{r}$ follows a Gaussian-random Markoff Process, Doob's First Theorem [50] inescapably determines the form of $g^{(1)}(\mathbf{q},\tau)$, namely: If $\Delta\mathbf{r}$ is a Gaussian Random Process, then the field correlation function is a single exponential with relaxation rate Dq^2. *Conversely, if the observed spectrum is not a single pure exponential, then* $\Delta\mathbf{r}$ *is not governed by a Gaussian-random Markoff process, and eq 10 is incorrect.* A non-exponential $g^{(1)}(q,\tau)$ could formally be written as a product of $\exp[-q^2\left\langle(\Delta\mathbf{r})^2\right\rangle/6]$ and a set of 'correction' terms, but the correction terms would dominate the expansion of $g^{(1)}(q,\tau)$.

Berne and Pecora's text [48] is sometimes incorrectly cited as asserting that eq 10 is uniformly correct for light-scattering spectra. Berne and Pecora obtain eq 10 by a correct path, but as they correctly emphasize in their text they are only treating particles whose motions follow the classical Langevin equation. For such particles, displacements during successive time intervals are uncorrelated.

In contrast, in systems with viscoelastic behavior, such as nondilute polymer solutions, the hydrodynamic equations have memory terms, and particle motions do not obey the

Langevin equation, though they may be described by some sort of generalized Langevin equation. For diffusing particles in viscoelastic fluids: Displacements over non-overlapping time intervals are correlated. The process governing $\blacksquare\mathbf{r}$ is not a Markoff process. Equation 10 does not apply. The mean-square particle displacement is not given by $\log[g^{(1)}(q,\tau)]/q^2$. Correspondingly, in a complex fluid the dependence of $\log[g^{(1)}(q,\tau)]/q^2$ on t cannot in general be used to determine a formal time-dependent diffusion coefficient.

2.3 Characterization of Light Scattering Spectra

How, then, are light scattering spectra of complex systems to be interpreted? Empirically, we find that spectra can be written as a sum of decay modes, each mode having the form of a stretched exponential in time

$$g^{(1)}(q,t) = \sum_{i=1}^{N} A_i \exp(-\theta_i t^{\beta_i}). \tag{11}$$

In this equation, the N modes are labelled by i; a stretching parameter β_i and decay pseudo-rate θ_i determine the temporal evolution of each mode; the mode amplitudes are the A_i. A stretched-exponential lineshape could also be parameterized as

$$g^{(1)}(q,t) = \exp(-(t/\tau_i)^{\beta_i}), \tag{12}$$

but noting $\theta_i = \tau_i^{-\beta_i}$ it is seen that the alternative form contains the same information as the form we used. θ_i is termed a pseudorate because it has dimensions 1/(time)$^{\beta_i}$. β_i is in general not an integer, and correspondingly θ_i depends on time to some non-integer power. In contrast, a true rate has dimensions time^{-1}.

How are the θ_i and the β_i related to the system dynamics? The mathematical properties of the field correlation function constrain the properties of θ_i and τ_i. Recall that $g^{(1)}(q,t)$ is determined by the (time-dependent) positions $\mathbf{r}_i(t)$ of the N scattering particles. In our experiments, the scattering particles were dilute, while the background polymer solution scattered relatively little light. In this case, the field correlation function simplifies to

$$g^{(1)}(q,t) = \left\langle \sum_{i=1}^{N} \exp(i\mathbf{q}\cdot(\mathbf{r}_i(t) - \mathbf{r}_i(0))) \right\rangle. \tag{13}$$

Here q is the magnitude of the scattering vector $\mathbf{q}$. The brackets $\langle \quad \rangle$ denote the ensemble average.

The constraints appear on making a Taylor series expansion in q of the exponential. Terms odd in the particle displacements vanish by reflection symmetry. The displacement of a probe from 0 to t is given by the integral of the probe velocity $\mathbf{v}_i(s)$ from 0 to t. Factoring constants outside averages, we find

$$g^{(1)}(q,t) = 1 - \frac{1}{2}q^2 \left\langle \int_0^t ds_1 \int_0^t ds_2 (\hat{q}\cdot\mathbf{v}_i(s_1))(\hat{q}\cdot\mathbf{v}_i(s_2)) \right\rangle +$$

$$\frac{1}{4!}q^4 \left\langle \int_0^t ds_1 \int_0^t ds_2 \int_0^t ds_3 \int_0^t ds_4 (\hat{q}\cdot\mathbf{v}_i(s_1))(\hat{q}\cdot\mathbf{v}_i(s_2))(\hat{q}\cdot\mathbf{v}_i(s_3))(\hat{q}\cdot\mathbf{v}_i(s_4)) \right\rangle - \ldots \tag{14}$$

The unit vector is $\hat{q} = \mathbf{q}/q$. Times, when invoked as variables of integration, are denoted s_i. If this expansion is convergent, $g^{(1)}(q,t)$ is a power series in q^2. The series coefficients may depend on t but do not depend on q.

Separate from the expansion in q in eq. 14, each stretched exponential of eq. 11 is readily expanded as a power series in the decay pseudorate θ. The decay pseudorate θ in turn has an expansion in q, that may be inserted into the power series in θ for eq. 11. An expansion of θ in terms of q does not have to correspond to eq. 14 on a term-by-term basis, but the two q-expansions must be consistent. However, every term of eq. 14 is an integer power of q^2. If the two series both converge, the lowest-order dependence of θ on q must be as q^{2n}, for n some positive integer giving the lowest nonzero nontrivial q-dependence of eq. 14. (We find experimentally $n = 1$.) Correspondingly, q enters τ in its lead dependence via $\tau = \theta^{-\beta}$, so τ depends on q via a noninteger power $q^{-2n/\beta}$.

This rationale, showing that $\theta \sim q^2$ (or some higher even power) and $\tau \sim q^{-2/\beta}$, cannot be confuted by a contradictory demonstration that τ should depend on q^{-2n} and not $q^{-2/\beta}$. The key step of such a demonstration would be a power series expansion of eq. 12 in powers of the inverse nominal time τ^{-1}, leading to a conclusion $\tau \sim q^{-2}$. However, β is in general a non-integer, and correspondingly eq. 12 does not have a Taylor expansion in τ because it is not analytic in τ.

The stretched exponential form provides an accurate but not necessarily unique representation for the field correlation function. The parameters θ_i and τ_i have the unattractive features that θ has the dimensions of time to a *noninteger* power β that is not the same in different spectra, while τ depends on q to a related noninteger power, that is also different in different spectra. The variation in β from spectrum to spectrum is not large, but one might reasonably prefer to have parameters whose relative numerical values for different spectra did not depend on the system of units in use.

Alternative characterizations of light scattering spectra are provided by the method of cumulants and by spectral time moments. Cumulants supply a uniform, convergent, description of any light scattering spectrum in terms of its initial slope and its initial time derivatives. However, for clearly multimodal spectra, a form that isolates each mode, such as a sum of few-cumulant expansions or stretched exponentials, is physically appealing. To characterize multimodal spectra, we instead introduced[31] the use of spectral time moments to describe each mode.

Spectral time moments are inspired by the simple exponential moment equation

$$M_n \equiv \int_0^\infty dt\ t^n\ \exp(-\Gamma t) = \frac{\gamma(1+n)}{\Gamma^{1+n}}. \tag{15}$$

In eq 15, Γ is the true decay rate of a pure exponential. The order of the moment M_n is n. The Gamma function is here denoted $\gamma(1+n) = n!$, the notation distinguishing the function $\gamma(1+n)$ and the decay rate Γ. For a pure exponential relaxation, $\Gamma = 1/M_0$ and $\Gamma^2 = 1/M_1$.

Recall that any spectrum that decays monotonically to zero has an expansion as a sum of exponentials:

$$g^{(1)}(t) = \int_0^\infty d\Gamma A(\Gamma) \exp(-\Gamma t). \tag{16}$$

Here $A(\Gamma)$ is a normalized amplitude associated with Γ. We have normalized A, namely

$\int_0^\infty A(\Gamma)d\Gamma = 1$. The time moments of $g^{(1)}(t)$ are therefore

$$M_n \equiv \int_0^\infty dt\, t^n g^{(1)}(t) = \int_0^\infty d\Gamma\, A(\Gamma)\frac{\gamma(1+n)}{\Gamma^{1+n}}. \tag{17}$$

The moments and decay rates are related by $M_n/n! \equiv \langle \Gamma^{-n-1} \rangle$, leading to a mean relaxation time (and zeroth time moment) $M_0 = \langle \Gamma^{-1} \rangle$.

There is a direct correspondence between cumulants and central moments, and between the spectral time moments and moments of A. Namely, for $n \geq 2$ one has for the central moments

$$K_n = \int_0^\infty d\Gamma A(\Gamma)(\Gamma - \bar{\Gamma})^n. \tag{18}$$

The first few central moments are the first few cumulants of A. The first cumulant is the initial slope $\lim_{t\to 0} d\log(g^{(1)}(t))/dt$ of $g^{(1)}$. Higher cumulants are higher logarithmic derivatives of $g^{(1)}(t)$ as $t \to 0$. The time moments M_n are the negative (Γ^n, $n < 0$) moments of A. Negative moments are only convergent if $A(\Gamma)$ is not too large at small Γ.

Time moments represent integral averages over $g^{(1)}(t)$. To determine spectral moments accurately, one must measure $g^{(1)}(t)$ accurately at long times. We avoided this difficulty in finding the time moments of $g^{(1)}(t)$ by replacing the measured $g^{(1)}(t)$ with its fit to a sum of stretched exponentials, and integrating the fitting functions analytically. Analytic integration of a stretched exponential shows

$$M_0 \equiv \int_0^\infty dt\ \exp(-\theta t^\beta) = \gamma(1+1/\beta)/\theta^{1/\beta}. \tag{19}$$

The mean relaxation time of a stretched exponential can thus be calculated from its decay pseudorate and stretching exponent. Because we determined M_0 from a fitted stretched-exponential, and not from the spectrum itself, challenges in measuring $g^{(1)}(q,t)$ at large t are avoided. In practice, θ and β are found to be anticorrelated, in the sense that photon-counting noise, that causes θ to be exceptionally large, simultaneously causes β to be particularly small, and vice versa. The integral average that generates M_0 tends to cancel out these correlations, so that determinations of M_0 have less noise than is observed in θ or in β separately.

At the price of assuming that the stretched exponential form for each mode is indeed correct out to very large times, we can use accurate measurements of the field correlation function at shorter times to infer stretched-exponential parameters and therefore M_0, without needing perfect measurements of $g^{(1)}(q,t)$ out to very large times. This price is no different formally than the usual price of applying the cumulant expansion, namely that in applying cumulants one must know accurately the baseline to which the spectrum is decaying.

Regardless of how we parameterize our spectra, we had to determine the parameters that most accurately characterize each spectrum. We used nonlinear-least-squares minimization based on simplexes to determine our fitting parameters. Fits to light scattering spectra are ill-poised, so the number of parameters that can be extracted from a light scattering spectrum is small. However, spectral relaxations here span more than six orders of magnitude in time, permitting stable fits to be made to a sum of several modes. Indeed, we found numerically that we could fit our spectra to a sum of two or three modes without causing

the fits to become numerically unstable. As a practical approach, we fit each spectrum repeatedly while trying different numbers of modes. In most cases, a sum of two or three stretched exponentials sufficed to describe spectra accurately. (Except for some early work with a more limited digital correlator, fits to single stretched exponentials did not describe our spectra well.) A nominal mean diffusion coefficient corresponding to each mode is

$$D = \langle \Gamma \rangle / q^2. \tag{20}$$

We do not claim that each mode must correspond to a distinct physical process in the system. Certainly, if the movements of particles were described by a Langevin-like equation containing several independent 'random' forces, each with its own memory function or corresponding friction factor, then in general the corresponding field correlation function would be a sum of independent relaxations, with each relaxation corresponding to motions induced by a distinct random force. However, the argument does not work in the reverse direction, so that a single physical process with a complex memory function could result in a field correlation function describable as a sum of several stretched exponentials.

It is probably the case that other few-parameter near-exponential functions could fit the observed lineshape. We did not make an extensive search for possible alternative functions. In the end, each parameterization embodies a representative relaxation time or rate for the mode, and a representative measure of the mode's deviation from single-parameter behavior.

3 Phenomenology

This section presents a phenomenological description of the dynamics of aqueous hydroxypropylcellulose, including the solution viscosity, static light scattering, quasi-elastic light scattering spectra of HPC: water, and optical probe measurements of HPC:water solutions.

3.1 Viscosity

The low-shear viscosity η of hydroxypropylcellulose solutions has been studied by Russo, et al.[51], Yang and Jamieson[52], Phillies, et al.[23], Phillies and Quinlan [25], and Bu and Russo[33]. The two sets of measurements of Phillies and collaborators are the most extensive in the range of relative viscosities ($1 \leq \eta_r \leq 4 \cdot 10^5$) covered, and included polymers with $139 \leq M_w \leq 1280$ kDa. Phillies, et al.[23] measured the temperature dependence of η, determining $\eta(c)$ at 10 C (good solvent conditions) and 39 C (near-pseudotheta conditions). Bu and Russo used a cone and plate viscometer to measure η of 300 kDa HPC at concentrations up to 39 g/L and frequencies up to 0.6 Hz, finding that shear thinning could be neglected in their systems.

There is agreement in the literature that the low-shear viscosity of HPC solutions increases approximately exponentially with polymer concentration. Note, e.g., Ref. [51], Fig. 1; Ref. [23], Fig. 4; and Ref. [25], Fig. 1. Ref. [23] was apparently the first to remark that, above some elevated molecular- and temperature-dependent polymer concentration c^+, the near-exponential concentration dependence of η was seemingly replaced with a power-law concentration dependence. For HPC molecules ranging from 93 to 1120 kDa, ref. [23]

found c^+ ranged from ≈ 40 g/L down to ≈ 5 g/L. Prior studies had focused on polymer concentrations modestly below c^+ at which the transition would not have been conspicuous.

The most thorough of our studies of $\eta(c)$ is described in detail in ref. [25]. In this work, viscosity measurements were made on HPC samples with nominal molecular weights of 300, 1000, and 1150 kDa, leading to data of Figure 1. HPC concentrations ranged from 0.04g/L up to 100, 40, or 40 g/L, respectively, with measurements being made at 55 to 70 concentrations for each polymer sample. The solution viscosities extended from the solvent viscosity up to $2-4\cdot 10^5$ cP. At the larger viscosities, flow times were hours long; shear rates were much lower than in capillary measurements on low-viscosity fluids. Furthermore, measurements on high viscosity liquids were repeated using different viscometers, with flow times differing five-fold, getting about the same η with both viscometers. It follows that shear thinning effects were not significant in these measurements.

In Figure 1, small triangles represent the measured data. For concentrations under 1.0 g/L, η increases slowly with increasing c. At higher concentrations, the rate of increase of η progressively accelerates, with $d\eta/dc$ increasing smoothly. At elevated concentrations, the plots of η against c fall along straight lines. From these graphs, at lower concentrations $\eta(c)$ follows a stretched exponential in polymer concentration,

$$\eta(c) = \eta_o \exp(-\alpha c^{\nu}), \tag{21}$$

seen in Figure 1 as smooth solid curves obtained from fits to the smaller-c points. Here η_o is the solvent viscosity, and α and ν are a scaling prefactor and a scaling exponent. At higher concentrations the viscosity shows power law behavior

$$\eta(c) = \bar{\eta} c^{x}. \tag{22}$$

Here $\bar{\eta}$ and x are a scaling prefactor and a scaling exponent, respectively. The straight lines represent least-mean-square fits to eq. 22.

The transition between the stretched-exponential and power-law regimes has several signal properties. The transition is sharp: Almost every data point (and as seen in Figure 1b, inset, we made measurements spaced close together in c to cover the transition region) lies on one curve or the other. Denoting the transition concentration c^+, even a modest change in c^+ from its optimal value greatly increases the mean-square error in the fits to eqs 21 and 22. The fitted stretched-exponential and power law curves are almost tangent. If the gap between the two curves is real, its width δc has $\delta c/c < 0.05$. Furthermore, the transition is analytic. Not only $\eta(c)$ but also the first derivative $\partial \log(\eta)/\partial \log(c)$ are continuous at the transition.

We term the $c < c^+$ stretched-exponential zone the 'solutionlike' regime and the $c > c^+$ power-law zone the 'meltlike' regime. These terms are *names*, chosen so that the reader can tag the associated phenomenologies without invoking terms (e.g., 'dilute', 'semidilute') entangled in associations with particular physical models for polymer dynamics. We emphasize that, in the meltlike regime, power-law behavior is actually visible in the data, over an extended range in c. This power-law behavior should be contrasted with asymptotic power laws never or barely reached in data, or with power-law tangents to data that in a log-log plot clearly lies on a smooth curve.

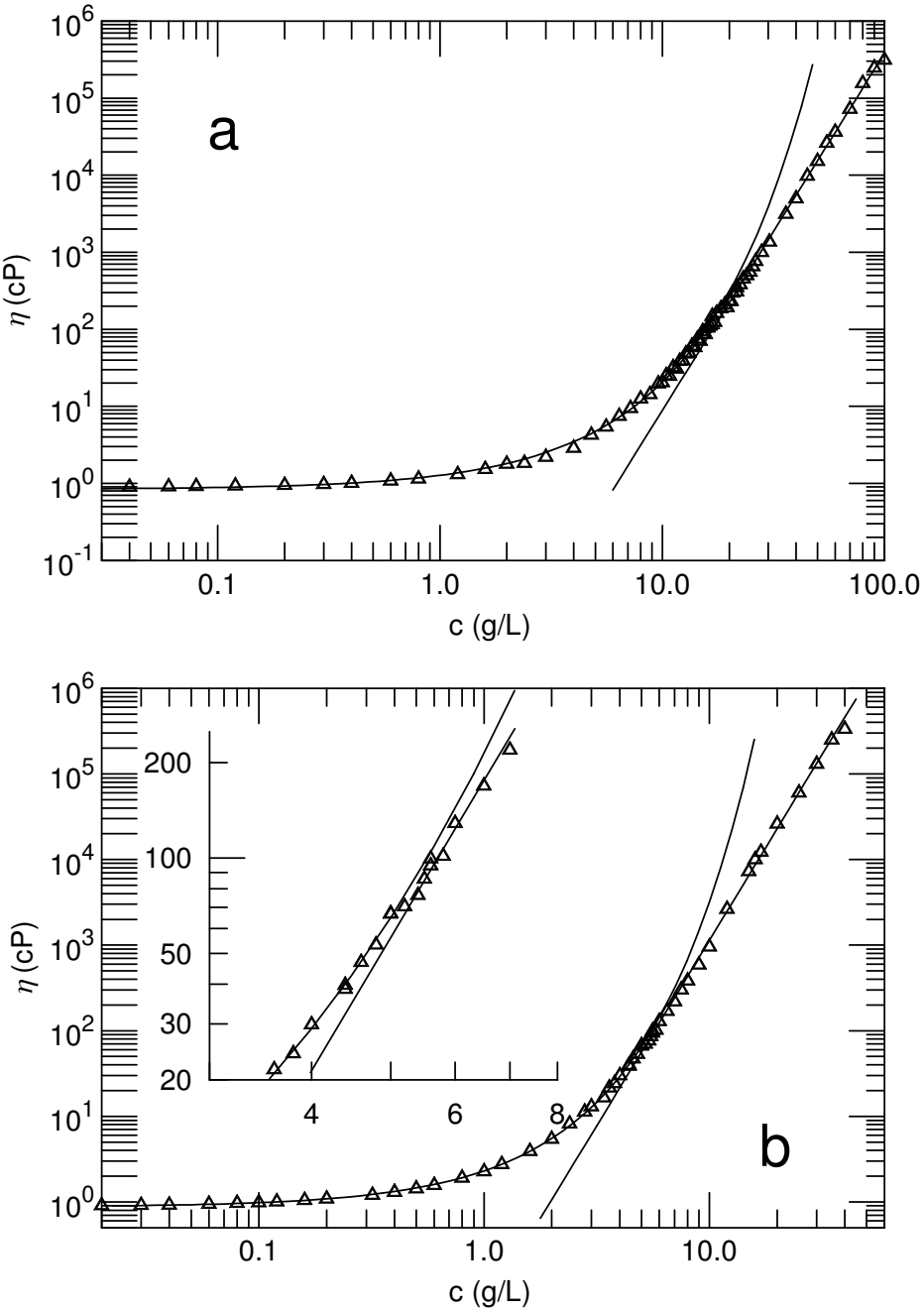

Figure 1: Viscosity against concentration of (a) 300 kDa, (b) 1 MDa, and (next page, top) (c) 1.15 MDa hydroxypropylcellulose:water, after Phillies and Quinlan[25].

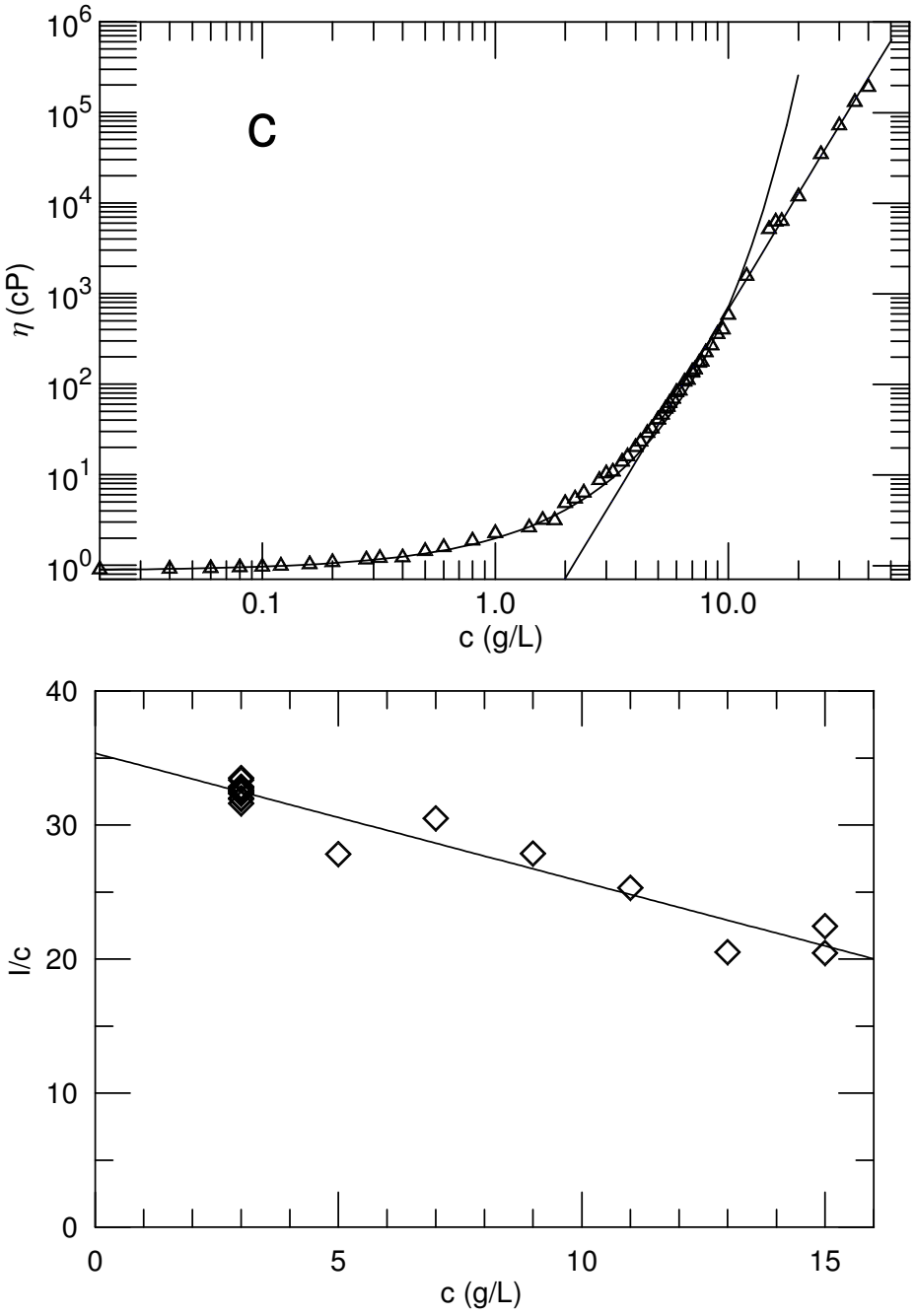

Figure 2: Normalized static scattering intensity I/c of aqueous 1MDa HPC, as a function of HPC concentration, and simple linear fit to I/c as a function of c, showing that the scattering per molecule of HPC in solution declines slowly but uniformly with increasing concentration, after O'Connell, et al.[59].

The solutionlike-meltlike transition is not unique to HPC solutions. A solution-like-meltlike transition was identified though not named by Lin and Phillies[53] in solutions of non-neutralized poly-acrylic acid:water. Solutionlike-meltlike transitions are apparent in data of Utracki and Simha on polydimethylsiloxane:pentadimethylsi-loxane[54] and of Takahashi, et al. on polystyrene solutions[55]. However, the solutionlike-meltlike transition is not universal. Utracki, et al.[54], also present parallel measurements on polyisobutene solutions, in which log-log plots of viscosity against reduced concentration uniformly lie on smooth curves, not straight lines, showing that a meltlike regime does not appear in these solutions.

It might hypothetically be proposed that the solutionlike-meltlike transition is (i) a precursor to the solution:liquid crystal phase transition exhibited by HPC:water solutions, or alternatively (ii) that the transition arises from dynamic behavior general to most polymers. However, the molecular weight dependences of the solutionlike-meltlike and liquid crystal phase transitions are quite different: In solutions of 93 or 1120 kDa HPC, c^+ is 40 or 5 g/L, respectively, so c^+ depends strongly on M. In contrast, the lyotropic transition of HPC occurs at a nearly molecular-weight-independent concentration[10], at concentrations far above those studied here[56]. Furthermore, Enomoto, et al.'s[57] results on η of the rodlike polymer schizophyllan argue against the correctness of either of these hypotheses: First, the phase transition concentrations of schizophyllans are much higher (100-200g/L) than the c^+ seen here. Second, at the liquid:biphasic phase boundary, the solution η of schizophyllan solutions falls dramatically, while in contrast at the viscosity transition concentration c^+ the HPC viscosity continues to increase. Third, non-linear least square fits to Enomoto, et al.'s measurements show that schizophyllan solutions remain in the solutionlike regime[58] (η a stretched exponential in c) at all concentrations and molecular weights studied up to the liquid:biphasic phase boundary (η/η_o as large as 10^4 or 10^5, molecular weights 128–4300 kDa, concentrations up to 4–200 g/L, all respectively). The absence of a meltlike regime for schizophyllan solutions, even with concentrations and molecular weights far into the regime in which HPC solutions show the transition, shows that the transition is not a universal property of semirigid rod polymers.

3.2 Static Light Scattering

One possible explanation for the solutionlike-meltlike transition is that the polymer forms clusters at concentrations $c > c^+$. The clusters, regions of unusually high density, would diffuse as semirigid bodies, whose hydrodynamic interactions and inability to interpenetrate would perturb the concentration dependence of the viscosity. To search for cluster formation, we (O'Connell, et al.[59]) examined static light scattering by 1 MDa HPC solutions in deionized ultrapure water at different concentrations, including concentrations on both sides of $c^+ \approx 6$ g/L. To perform these measurements, HPC solutions were made at a series of concentrations ranging up to 15 g/L. Samples were passed into light scattering cells through 1.2μ pore diameter nanoporous filters (this being the smallest pores through which the most concentrated solutions could be persuaded to pass) and allowed to stand for a day. Samples were then placed seriatim into the path of an argon laser beam. The photocount rate at a photomultiplier tube detector was then integrated for 30 second intervals, with the experimenter alternating between new samples and a given baseline sample, and with the

background intensity measured with a sample containing only pure water being measured and subtracted.

The outcome of the measurements appears in Figure 2, which shows the intensity I in its normalized I/c form. $[\eta]^{-1}$ of this system is about 1.4 g/L. We limit data shown here to concentrations above $[\eta]^{-1}$, but have results for a series of concentrations between $[\eta]^{-1}$ and c^+. The normalized scattering intensity is seen to decline slowly with increasing polymer concentration. There is no suggestion of a discontinuity or change, near c^+, in the slope of I/c against c.

3.3 Quasi-Elastic Light Scattering by HPC

Light scattering spectra were obtained[59] of aqueous solutions of 1MDa HPC for concentrations in the range 0.5-15 g/L. This range of concentrations spans c^+ and includes a substantial number of solutions having concentrations well below and well above the solutionlike-meltlike transition.

Representative spectra and fits appear in Figure 3. At HPC concentration 1 g/L, the spectrum has a single visible decay centered around 10^3 μS. At 4.5 g/L, a weak slower mode is visible. At 7 g/L HPC, the spectrum gains an additional relaxation whose decay occurs at times $> 10^4$ μS. With increasing concentration the slow decay becomes slower and more intense. At 12 g/L HPC, the slow decay almost entirely dominates the spectrum.

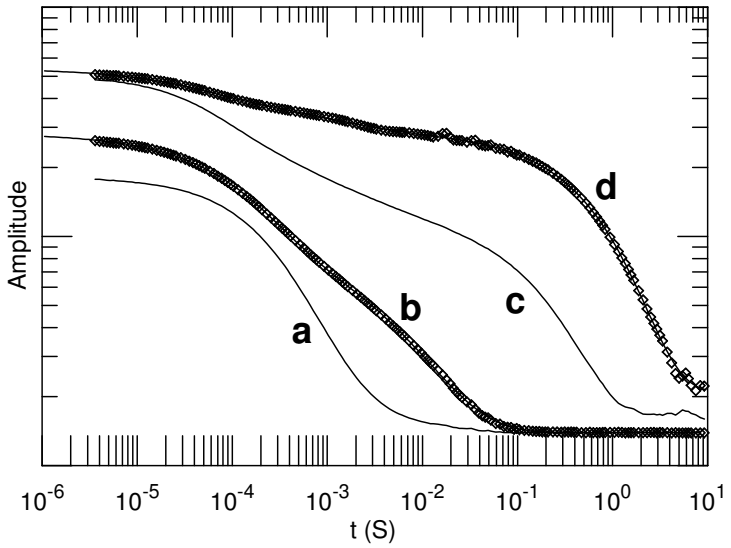

Figure 3: Renormalized spectra $S(q,t)$ of aqueous solutions of 1MDa HPC at concentrations of (a)1, (b) 4.5, (c) 7, and (d) 12 g/L HPC. At 4.5 and 12 g/L, points are data and line are fits to two or three stretched exponentials, respectively. For readability, these spectra were renormalized and displaced vertically relative to each other.

By fitting each spectrum to eq 11, with 1, 2, or 3 relaxational modes assumed, quantitative descriptions of all spectra were obtained[59]. In the solutionlike regime, the single

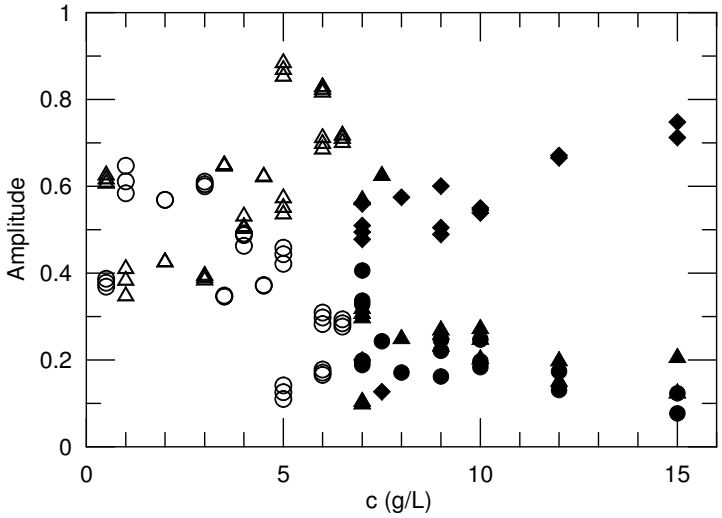

Figure 4: Relative amplitudes of the fast (circles), intermediate (triangles), and slow (diamonds) spectral modes of HPC:water as functions of HPC concentration. Open points indicate parameters from two-mode fits; filled points indicate parameters for three-mode fits.

visible relaxation of HPC:water spectra is described well by a sum of two stretched exponential modes; these spectra are not fit well by a single stretched exponential. Near c^+, spectra gain a further, very slow spectral relaxation, with three distinct stretched exponential modes being required to describe the spectrum; fits to two stretched exponentials lead to curves that do not describe the data accurately. The fitting parameters corresponding to the various modes differ from each other substantially; the amplitudes of two or three modes differ from each other by no more than a factor of two. When the spectral moments M_0 of the modes are close, the corresponding stretching exponents and hence the mode lineshapes are extremely different. Challenges to accurate fitting, that appear when single exponentials have linewidths differing by a factor of two or less, or that appear when some modes are much weaker than others, do not arise here.

The relative amplitudes of the modes are shown in Figure 4. Below c^+, there are two amplitudes, one each for the intermediate and for the fast mode; above c^+, there is also an amplitude for the slow mode. At lower concentrations, the fast and intermediate modes have approximately equal amplitudes. Just below c^+, the intermediate mode briefly dominates. Above c^+, half or more of the total amplitude is transferred to the slow mode; the remainder of the amplitude is shared approximately evenly between the fast and intermediate modes. At the lowest concentrations at which the slow mode is apparent, it already forms the largest single part of the spectrum. Static light scattering measurements show that the total scattering intensity does not increase near c^+. The changes in relative spectral amplitudes here thus reflect the transfer of scattering intensity out of established modes, and into a new mode, not the appearance of additional scattering in a new mode without diminishing the scattering into the pre-existing fast and intermediate modes.

Figure 5 gives gives the effective diffusion coefficients corresponding to the fast, inter-

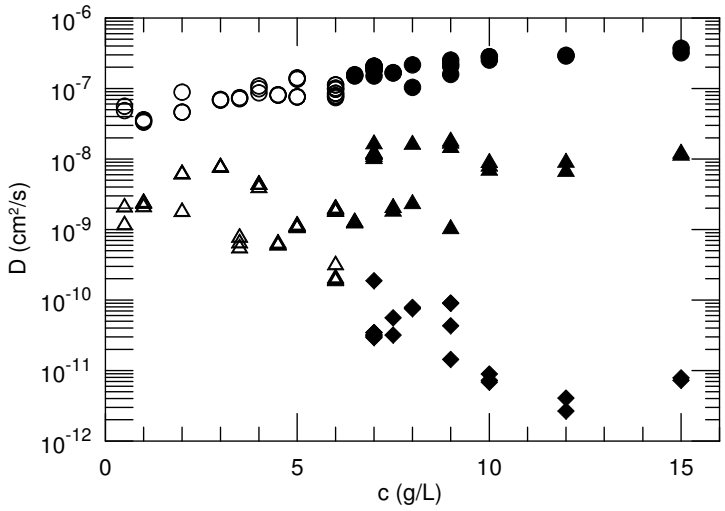

Figure 5: Effective diffusion coefficients $D = \langle\Gamma\rangle/q^2$ fast (circles), intermediate (triangles), and slow (diamonds) spectral modes of HPC:water. Open and closed points indicate parameters from two- and three-mode fits, respectively.

mediate, and slow modes, using eq 20 to convert the average decay rate $\langle\Gamma\rangle$ to D, based on data of O'Connell, et al.[59]. Over the observed range of concentrations, the diffusion coefficient of the fast mode increases from $\sim 4\cdot10^{-8}$ to $3\cdot10^{-7}$ cm^2/s, with no indication of an anomaly near the transition concentration c^+. Over the same concentrations, the diffusion coefficient corresponding to the intermediate mode also increases perhaps five-fold, starting near $2\cdot10^{-9}$ and reaching $\sim 1\cdot10^{-8}$ cm^2/s at the largest concentration studied. At all concentrations, the diffusion coefficients of the fast and intermediate modes remain separate by at least an order of magnitude, indicating that there should be no difficulty in resolving these modes during the numerical fitting process. The slow mode is inapparent below 6 g/L. When first observed, the slow mode's diffusion coefficient is about $1\cdot10^{-10}$, falling to $\sim 3\cdot10^{-12}$, cm^2/s in the most concentrated HPC solutions. Near 6 g/L, the diffusion coefficients of the intermediate and slow mode approach each other, leading to challenges in resolving the two modes. Indeed, in the concentration range 5-6/L, these two modes cannot be resolved, and D of the one resolved mode is substantially less than D of the intermediate mode as observed at smaller or larger concentration. While there are precursor effects at lower concentrations, the slow mode can first be resolved from the intermediate mode at concentration c^+.

Ref. [59] appears to be the only systematic study of QELSS spectra of HPC:water. However, the first observation of an HPC slow mode, present only in spectra of concentrated solutions, is properly credited to Russo, et al.[51], who note without quantitation a HPC:water spectral mode that "...decays at an exceptionally slow rate."

3.4 Optical Probe Studies of HPC Solutions

In an optical probe study of a polymer solution, dilute, intensely-scattering or fluorescent probes are added to the solution. QELSS, FRAPP, or other means are used to monitor

the diffusion of the probes, which may be small molecules, colloidal particles, or polymer chains. The dynamics of the diffusing probes are used to infer the dynamics of the polymer solution.

3.4.1 Early Work

Applications of optical probe diffusion to HPC solutions include studies by Brown and Rymden[62], Russo, et al.[51], and Yang and Jamieson[52]. Brown and Rymden studied 72nm radius latex spheres diffusing through hydroxypropylcellulose, hydroxyethylcellulose, and carboxymethylcellulose, showing that scattering by the latex dominated scattering by any of the polymers, that HPC binds to the surface of the latex particles creating clusters of bridged particles, and that addition of Triton X-100 tends to alleviate the effects of polymer adsorption on probe diffusion.

Russo, et al.[51] examined the diffusion of 79 and 181nm diameter latex spheres through aqueous 292 kDa HPC. They demonstrated that the latex spheres bind HPC, but the adsorption is reversible; addition of a trace of the nonionic surfactant Triton X-100 is sufficient to abolish HPC adsorption by the probes. Russo, et al., using a 272 channel correlator, found that their probe spectra were not greatly nonexponential over the first two decades of decay, with a variance (normalized second cumulant of the spectrum) that remains roughly the same at most polymer concentrations up to $\approx 40g/L$. The diffusion coefficient of the probes showed a stretched-exponential concentration dependence

$$D = D_o \exp(-\alpha c^{\nu}). \tag{23}$$

Here D_o is D at zero concentration, and α and ν are a scaling prefactor and exponent. In the absence of Triton X-100, complications in applying this form arose because one encounters cluster formation at relatively low polymer concentrations. The apparent diffusion coefficient varies with c because it corresponds to objects of inconstant size. However, on sorting out the diffusion coefficient due to clusters, Russo, et al. found that the microviscosity η_μ, inferred from the diffusion coefficients of the clusters, tracks well the viscosity measured macroscopically. For surfactant-coated spheres (cluster formation suppressed) and HPC concentrations up to 10 g/L, η_μ and η were found to agree to within 12%.

Yang and Jamieson[52] used QELSS to examine 120, 210, and 350 nm polystyrene latex spheres diffusing through solutions of four HPC samples. Triton X-100 was used to suppress polymer binding. Polymer molecular weights M_w were determined from static light scattering to be 110, 140, 450, and 850 kDa. Relative viscosities η_r ranged up to 10-45 depending on the M_w studied. With the two lower-molecular-weight polymers, $\eta \approx \eta_\mu$ was found. In solutions of the 450 kDa polymer, η_μ/η declined from 1.0 to ≈ 0.3 with increasing c. η_μ/η increased with increasing sphere size, but, in solutions of the 450 and 850 kDa HPC, Yang and Jamieson found $\eta_\mu/\eta < 1$ even for 350nm diameter spheres. Yang and Jamieson further found that D follows approximately a stretched-exponential concentration dependence, but with a low-concentration near-plateau, which they described functionally as $D = D_o$ for $c < c_y$ and $D = D_o \exp(-\alpha(c^{\nu} - c_y^{\nu}))$ for concentrations $c > c_y$.

Building on these early results, we made an extremely extensive study of optical probe diffusion in HPC solutions. We varied systematically the probe radius, polymer concentration, scattering vector, and temperature. We also obtained limited data on the effect of

polymer molecular weight. From these results, we obtained a coherent picture of probe diffusion in aqueous hydroxypropylcellulose solutions.

Most of our results were obtained for probes diffusing through solutions of nominal 1MDa HPC (Scientific Polymer Products) to which 0.2 wt% Triton X-100 was added to prevent HPC adsorption by the probes. The Triton X-100 concentration was based on preliminary studies showing that the diffusion coefficient of polystyrene spheres in HPC:water increases markedly over a narrow range of Triton X-100 concentration, but is substantially independent of Triton X-100 concentration outside of this range. This transition may be identified as the adsorption of HPC by the spheres being reversed by surfactant, as described by Russo, et al.[51]. We chose a fixed Triton X-100 concentration that was appreciably above the Triton X-100 concentration required for polymer desorption.

Our probe particles were carboxylate-modified polystyrene latex spheres with nominal diameters 14, 21, 35, 38, 50, 67, 87, 189, 282, 455, and 760 nm. Extrapolating from the results of Yang and Jamieson[52] we estimate that the 1MDa HPC had a diameter of gyration $2R_g \approx 210$nm and a hydrodynamic diameter $2R_h \approx 110$nm, so our probes ranged from substantially smaller to substantially larger than the HPC molecules.

Our[27]-[31] light scattering spectrometers featured an argon-ion or frequency-doubled diode laser operating in the green, a BI-2030 or ALV multi-tau digital correlator, temperature stabilization to 0.1C, and optical trains with a 90^o scattering angle or a rotating goniometer arm covering $28^o \leq \theta \leq 107^o$. Probe spectra were fit at the field correlation level to a sum of two or three stretched exponentials. Fits to a single stretched exponential in time were uniformly unsatisfactory; when two (or three) stretched exponentials were needed, experimental fits to three (or two) stretched exponentials were not satisfactory. In practice, fits to two stretched exponentials were satisfactory for all probes for $c < c^+$. For concentrations $c > c^+$, larger spheres (50nm and larger diameters) clearly gave bimodal spectra, but 35nm spheres (the only small probes studied for $c > c^+$) unambiguously had trimodal spectra at elevated polymer concentrations.

A variety of control experiments were used to test whether probe spectra were contaminated by light scattering spectra of the HPC itself. Spectra of probe:polymer mixtures and of probe-free polymer solutions were measured under identical conditions (same laser power, iris settings, and photomultiplier tube voltages) for equal integration times. The probe-free solution spectra had a small fraction (1-4%) of the amplitude of the probe-containing spectra. Fits were also made to spectra of probe-containing solutions, and to the same spectra after subtraction *at the field correlation function level* of matching control spectra of the corresponding probe-free polymer solutions. The effect of spectral subtraction on the fitting parameters was substantially less than the random fluctuations in the fitting parameters from spectrum to spectrum of a single solution. Finally, selected control experiments were made by tripling the probe concentration, finding that the spectral amplitude increased approximately threefold without change of shape, showing that we were observing probe spectra.

Our primary effort in Ref. [28] was a systematic exploration of concentrations $c < c^+$, which revealed the fundamental length scale governing probe diffusion in the solutionlike regime. We then in Ref. [29] examined how larger probe particles diffuse in more concentrated ($c > c^+$) solutions, showing that at $c \approx c^+$ there is a dramatic change in the concentration dependence of the spectral lineshape parameters, thereby confirming the reality of

the solutionlike-meltlike viscosity transition. Finally, in Ref. [31] we examined how a small probe species diffuses in the meltlike $c > c^+$ regime, and introduced time moments as an alternative description for spectra. Associated studies give information on the dependence of probe diffusion on polymer molecular weight and on temperature (equivalently, solvent quality). As shown in the discussion, these approaches lead to a coherent description of diffusive modes in HPC solutions, allowing us to identify the dominant length scale for polymer solution dynamics as the radius of an entire polymer chain.

3.4.2 Probe Diffusion in the Solutionlike Regime

Spectra of optical probes in HPC: water for polymer concentrations $c < c^+$ are naturally divided into two classes, namely spectra of small probes (diameter $d \leq 67$ nm) and of large probes ($d \geq 67$ nm), with the 67 nm spheres showing some properties of each class. We only had probes with a limited number of diameters. Consequently, we can only say that the small probe-large probe boundary is someplace between 50nm (definite small-probe behavior at concentrations below c^+) and 87 nm (definite large-probe behavior for $c < c^+$). With increasing c, the small/large probe boundary moves slightly, so near c^+ the 50 and 67nm spheres shift from small- to large- probe behavior. Spectra of small spheres are obviously bimodal at all non-zero polymer concentrations that we studied. Spectra of large spheres do not show two obvious, well-resolved modes, but numerical fitting revealed their bimodal nature: A single stretched exponential did not fit these spectra well, but the sum of a stretched exponential and a pure exponential did. (Large-sphere spectra could also be fit by the sum of two stretched exponentials, but for one mode β was approximately unity, and for both modes the fitting parameters were somewhat scattered with θ_s not showing a clean q^2 dependence. In contrast, the fit to the sum of a stretched exponential and a pure exponential gave stable values for the fitting parameters, while the relaxation rate of the pure exponential scaled diffusively, i.e., linearly with q^2.) For the intermediate 67nm spheres, we reported two sets of parameters, namely parameters describing a fit to a sum of two stretched exponentials and alternatively a fit to the sum of a stretched exponential and a pure exponential.

We denote the two modes as the *sharp* mode and the *broad* mode, and denote parameters relating to these two modes by subscript s and subscript b, respectively. The sharp mode is either a pure exponential (large spheres; $\beta_s = 1$) or nearly a pure exponential (small spheres; $1 \geq \beta_s \geq 0.7$). The broad mode has an appreciably smaller β than does the sharp mode, namely $0.9 \geq \beta_b \geq 0.6$ for large spheres and $0.6 \geq \beta_b \geq 0.2$ for small spheres. In our earlier papers, these two modes were referred to as the 'slow' and 'fast' modes. However, depending on sphere size and polymer concentration, the 'fast' mode may decay either sooner or later than the slow mode, so we replaced the slow/fast nomenclature with the sharp/broad nomenclature.

Figures 6a and 6b show the stretching parameters β_s and β_b as functions of matrix polymer concentration for each sphere size, including $c > c^+$ data discussed later. For large spheres, β_s is unity. For small spheres ($14 \leq d \leq 67$nm), β_s falls progressively with increasing polymer concentration. For all spheres, β_b falls with increasing c until c^+ is reached, while the slope $d\beta_b/dc$ is approximately the same for small and for large spheres. Above c^+, β_b is nearly independent of c.

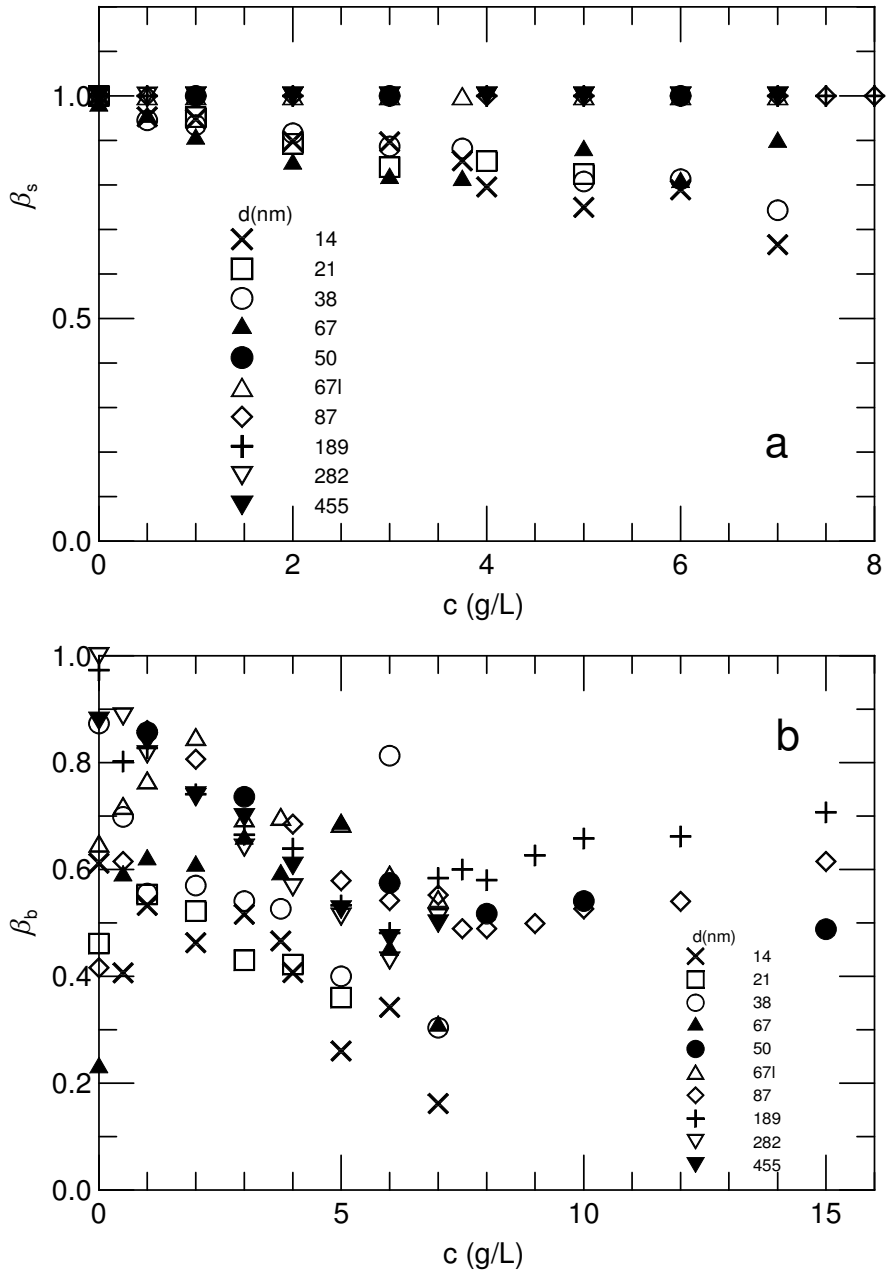

Figure 6: Spectral parameters from optical probe spectra. Stretching exponents a) β_s and b) β_b of the sharp and broad modes, obtained by fitting the spectra of small ($d \leq 67$nm) probes to a sum of two stretched exponentials and fitting the spectra of large ($d \geq 67$nm) spheres to the sum of a stretched exponential and a pure exponential (for which $\beta_s = 1$ applies). Fits to 67nm sphere spectra are reported treating it both as a small "67" and as a large "67l" probe. For $c > 8g/L$, only large spheres for which $\beta_s \equiv 1$ (not plotted) were studied.

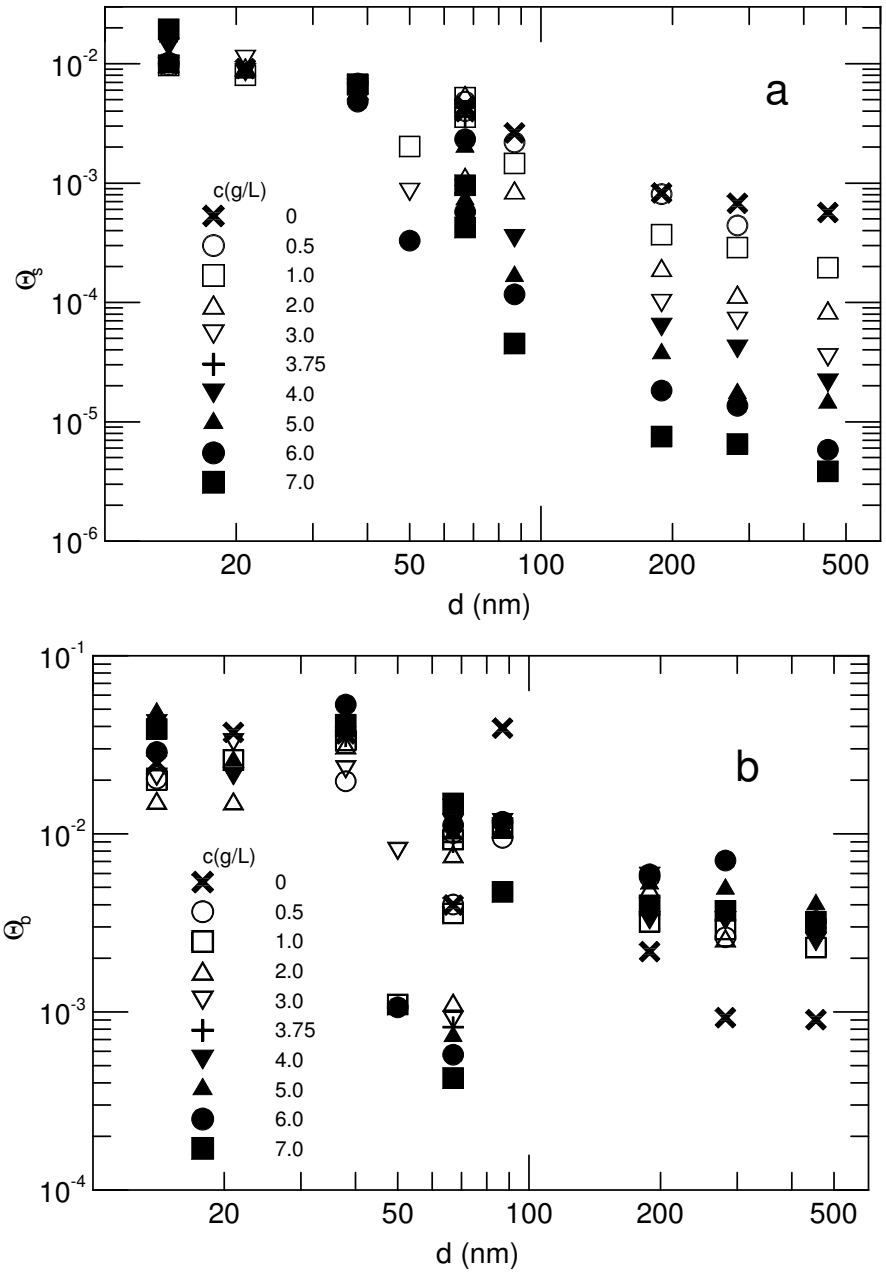

Figure 7: Relaxation pseudorates a) θ_s and b) θ_b of the sharp and broad modes, respectively, plotted as functions of probe diameter at each of a series of polymer concentrations $c \leq c^+$, showing showing the marked difference in concentration dependences between small ($d <$ 50nm) and large ($d >$ 50nm) sphere behavior.

Figures 7a and 7b show the relaxation pseudorates θ_s and θ_b, as functions of probe diameter, at each of a series of concentrations. d spans a factor of 30 in probe size, from 14 to 455 nm. θ_s falls monotonically with increasing sphere diameter. However, there are marked differences between small and large probes. For each small probe, θ_s is nearly independent of c for $c < c^+$. For large spheres, θ_s depends strongly on c. This difference between small and large probes has also been seen by Bu and Russo[33] as discussed below. In contrast to θ_s, for small spheres θ_b is substantially independent of probe diameter, while for large spheres θ_b falls markedly with increasing d.

The concentration dependences of θ_s and θ_b for each probe diameter appear in Figures 8a and 8b. For small spheres, θ_s is nearly independent of c. With increasing sphere diameter, θ_s decreases with increasing c, the decrease being steeper for larger spheres. For each sphere diameter, θ_s depends on c via a stretched exponential

$$\theta_s(c) = \theta_o \exp(-\alpha c^\nu). \tag{24}$$

Here θ_o is an intercept, while α and ν are a scaling prefactor and exponent, respectively. Except for the two largest spheres, $\nu \approx 1$. With increasing sphere size, α increases progressively by approximately 100-fold, from ≈ 0.01 for the 21 nm probes to 1.12 for the 455 nm probes.

In contradistinction to θ_s, the broad relaxation pseudorate θ_b is somewhat scattered. For $c < c^+$, θ_b does not have a strong monotonic concentration dependence for any size of sphere. At concentrations above c^+, θ_b declines markedly with increasing c, θ_b for the largest probes falling 20-fold between 6 and 15 g/L HPC. Random errors in θ and β are visibly anticorrelated; if one variable is especially large relative to neighboring points, the other is especially small.

Figure 9 shows the relative importance of the sharp and broad modes for small (14nm), intermediate (67nm), and large (455nm) spheres as functions of concentration. The importance of the broad mode increases with increasing concentration. The mode has next-to-no-amplitude at low concentration ($< 1g/L$) or large scattering angles. At concentrations above 2 g/L for small spheres and 90^o scattering, the sharp mode dominates the spectrum, with the broad mode amounting to 10-20% of the total amplitude. As seen below, the dominant mode for each probe size is the shorter-lived mode. For large probes, especially in nondilute solutions, the broad mode includes slightly more than half the total amplitude. Small probes in the meltlike region have a more complex mode structure discussed below.

3.4.3 Confirmation of the Reality of the Solutionlike-Meltlike Transition

In more recent work[29], probe diffusion in more concentrated solutions of 1MDa HPC was examined. The underlying motivation was to determine whether the solutionlike-meltlike rheological transition is a real physical phenomenon, or whether it is a mathematical artifact of the fitting process. The transition manifests itself[25] as a sharp change in the functional dependence of η on c. However, Ref [25]'s interpretation of their data is not unique. For example, the data could be interpreted as a series of power-law domains of progressively increasing slope, linked by somewhat-broad crossovers, with a final crossover transitioning at c^+ into the highest-concentration domain. Under this interpretation, the stretched-exponential concentration dependence is simply a numerical approximation that

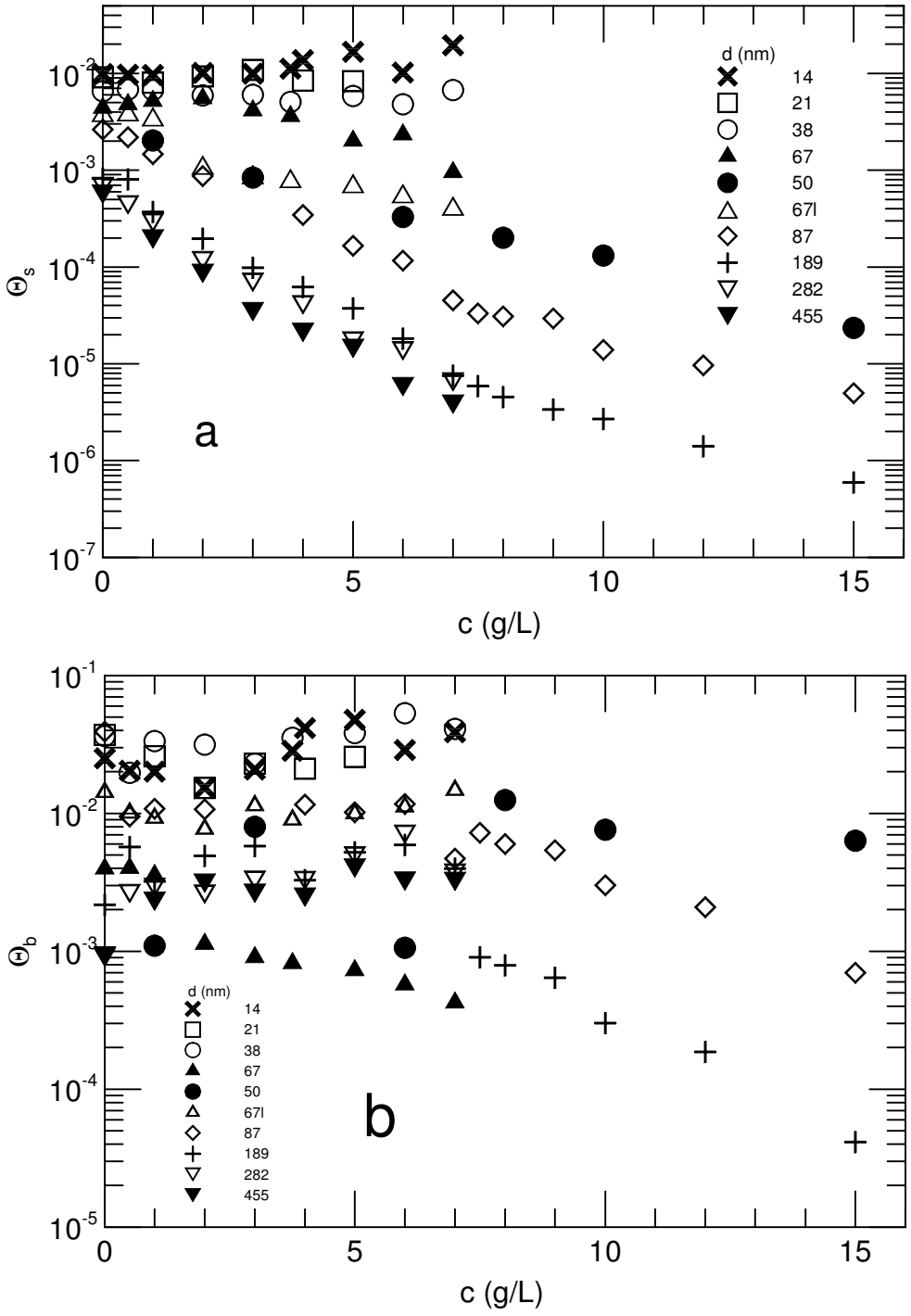

Figure 8: Relaxation pseudorates a) θ_s and b) θ_b plotted as functions of polymer concentration for each diameter of probe. For θ_s, the sensitivity to polymer concentration is markedly stronger for large probes than for small probes. For all spheres, θ_b is insensitive to polymer c until c^+ is reached. Above c^+, θ_b falls markedly with increasing c.

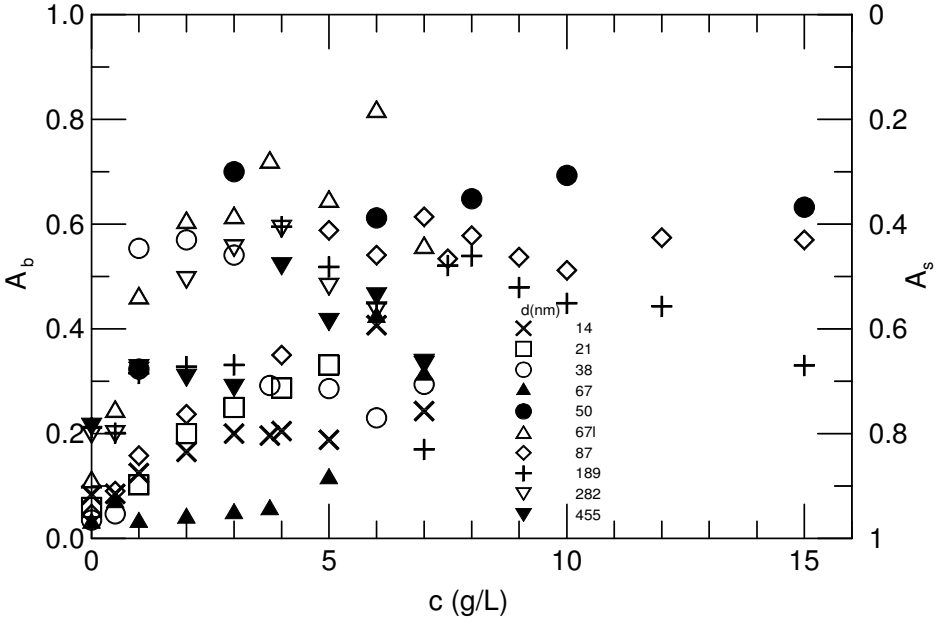

Figure 9: Relative amplitudes ($A_b + A_s = 1$ constrained) of the broad (left scale) and sharp (right scale) modes for 14-455nm probes (Figure legend) as functions of polymer concentration c.

has no physical significance, and c^+ is one border of one of several crossover regimes, not something of unique physical importance. We[29] expected that a comparison of probe behavior in solutionlike and meltlike solutions might speak to the reality of the solutionlike-meltlike transition, an expectation that proved justified by experiment.

We examined the diffusion of 50, 87, and 189nm probes in solutions of 1MDa HPC at concentrations up to 15g/L. For $c > c^+$, these are intermediate and large probes. Spectra of these probes were fit well by the sum of a pure exponential and a stretched exponential. Relaxation times extended from a few microseconds to a few seconds. To observe these spectra accurately, measurements of $S(q,t)$ covered almost seven orders of magnitude in time and several hundred to a thousandfold decay in spectral amplitude. For probes in the most concentrated samples, single experiments used up to 25hr integration times.

The concentration dependences of the lineshape parameters θ_b, β_b, and A_b change dramatically at c^+. The decay pseudorate θ_s of the sharp mode shows a more modest transition at c^+. Figures 8b and 6b (above) show the concentration dependences of θ_b and β_b, respectively, for the 50, 87, and 189nm probes.

Consider first θ_b, as seen in Fig 8b. At concentrations up to 6 g/L, θ_b is substantially independent of polymer concentration. At concentrations above c^+, θ_b falls dramatically with increasing c. The extent of the decrease depends on probe diameter. Between 6 and 15 g/L HPC, θ_b of the 50nm probes falls almost twofold, but θ_b of the 189nm spheres declines nearly 100-fold. For $c > c^+$, the concentration dependence of θ_b may be represented as an exponential or power law in c. With the two smaller probes, the exponential fits the $c > c^+$ data somewhat better than the power law does. For the 189nm probes, the stretched-

exponential and power-law forms give approximately equally good descriptions of $\theta_b(c)$. When $q \to 0$, we find that $\theta_b \to 0$. In the meltlike regime $\theta_b(q)$ lacks the more complicated dependence on q seen in the solutionlike regime.

As seen in Fig 6b, below the transition concentration the stretching exponent β_b falls markedly with increasing c, from close to unity at low polymer concentration down to $\beta_b \approx 0.5$ in the concentration range 6-8g/L. Above the transition concentration, β_b of the intermediate size 50nm spheres ceases to change, while β_b of the 87 and 189 nm probes increases again from its lower limit of 0.5. For large probes β_b is substantially independent of scattering vector q.

Figure 9 shows how the amplitudes of the sharp and broad modes change as polymer concentration is increased. For all probes, below c^+ the amplitude of the broad mode increases from a low level until it is approximately half of the field correlation function. Near c^+, A_b ceases to increase; above c^+, $A_b \approx 0.5$. Above c^+, A_b depends weakly on probe size, being modestly less for the 189nm probes than for the 50nm probes. At elevated concentrations $c > c^+$, the relative amplitudes A_b and A_s are independent of scattering vector q.

Figure 8a shows θ_s at elevated concentrations. For the intermediate 50nm probes, a single stretched exponential in c describes $\theta_s(c)$. For the 87 and 189nm probes, $\theta_s(c)$ is better fit by two separate curves, one each for $c < 8$g/L and for $c > 8$g/L. Measurements on large probes find that θ_s scales accurately as q^2, with $\theta_s \to 0$ as $q \to 0$, consistent with θ_s being a simple diffusive transport coefficient.

It appears fruitful to compare the concentration dependences of the decay pseudorates and the solution viscosity η. This comparison appears in Figure 10, which plots $\theta_s\eta$ and $\theta_b\eta$ against c. Over the entire concentration range, $\theta_s\eta$ increases progressively with increasing c, by about four-fold for the 189 nm probes, but by perhaps 60-fold for the smaller 50nm probes. The concentration dependence of $\theta_s\eta$ differs little between $c < c^+$ and $c > c^+$. In contrast, the concentration dependence of $\theta_b\eta$ changes dramatically near c^+. Over $0 \le c \le 6$ g/L, for each probe $\theta_b\eta$ increases by about two orders of magnitude, corresponding to the hundred-fold increase in η and nearly-concentration-independent θ_b. At $c > c^+$, $\theta_b\eta$ increases much more slowly with increasing c, the increase being largest for the 50nm spheres and quite small for the 187nm probes.

We[29] thus find that concentration dependences of spectral lineshape parameters of large optical probes differ markedly between the solutionlike and meltlike concentration regimes. Furthermore, the concentration dependences change over a narrow concentration range centered on the viscometric transition concentration c^+. The experimental viscometric transition is thus echoed by measurements using a second, physically-independent experimental technique. Our results[29] thus support the conclusion that the solutionlike-meltlike transition is a real physical effect.

3.4.4 Relaxation Time Scales

It is sometimes proposed that deviations from simple-fluid behavior are a short-time phenomenon, but that at longer times transient viscoelastic effects will disappear, with the probe diffusion coefficient of large probes satisfying the Stokes-Einstein equation. To examine this question and compare probe spectra with spectra of polymer solutions, Phillies,

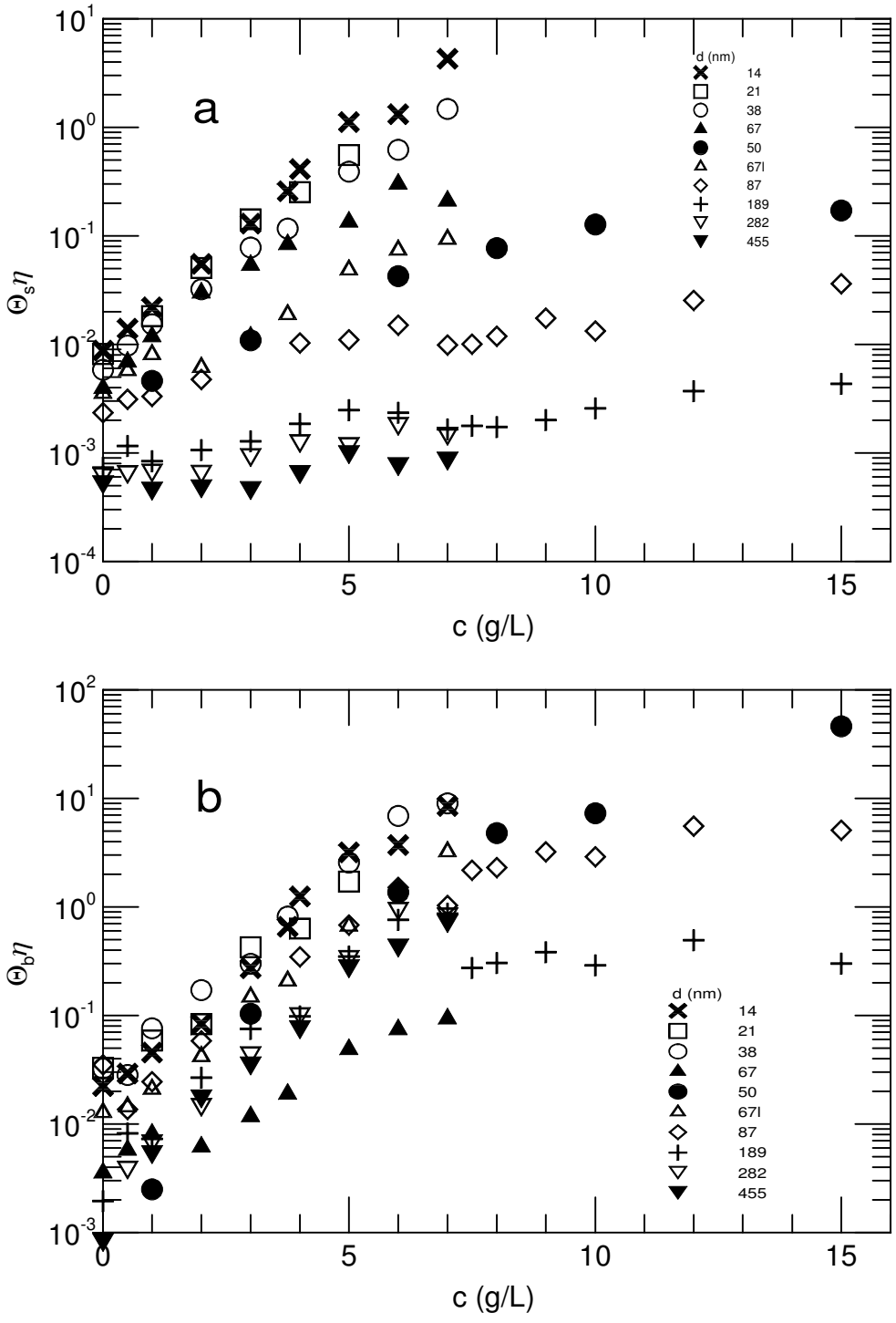

Figure 10: Correlation between decay pseudorates and the solution viscosity, from a) $\theta_s\eta$ and b) $\theta_b\eta$ against concentration for all probes studied.

et al.[31] used spectral time moments to re-analyze their earlier data. M_0 was recalculated for all probe:polymer combinations studied by Streletzky, et al., using θ_i and β_i previously determined[28]-[31]. Ref. [31] also studied diffusion of small (35 nm) probes in concentrated 1MDa HPC:water.

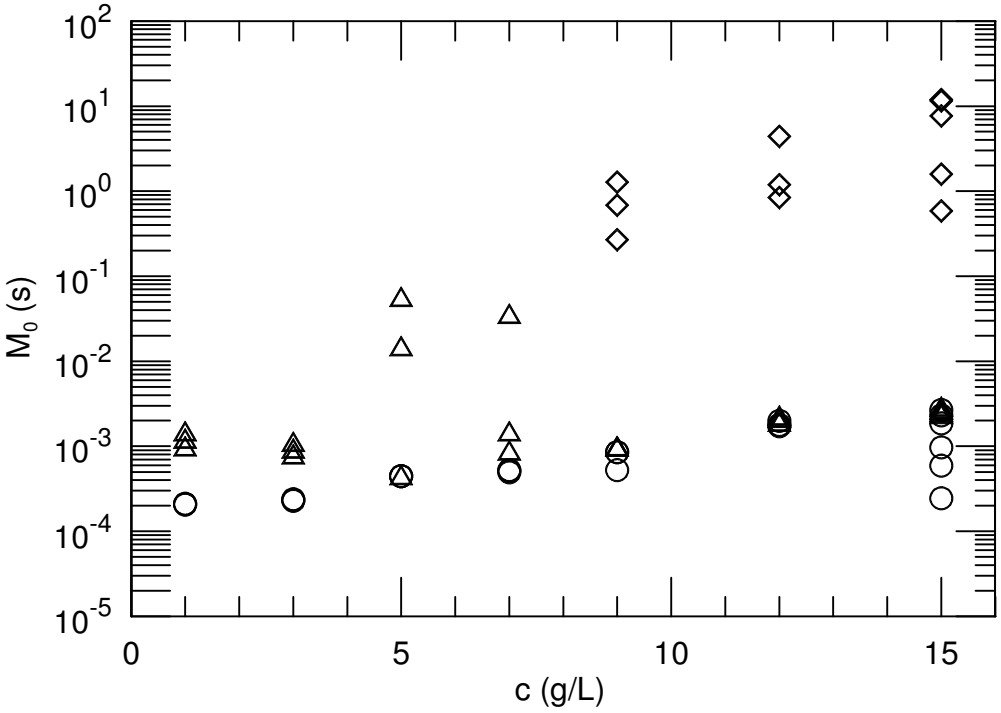

Figure 11: M_0 against c for the sharp (circles), broad (triangles), and ultraslow (diamonds) modes of 35 nm probes in HPC:water.

Time moments give a new perspective on the spectral modes. We originally characterized modes as 'slow' and 'fast' based on their initial slopes, effectively, their stretching exponents β. While this characterization is true, it is incomplete. The time moment perspective shows that the slow and fast modes are better termed *sharp* and *broad*, respectively, denoted by subscripts s and b, respectively. The sharp mode has β_s near 1.0; the broad mode has β_b closer to 0.5. For large probes at lower concentrations, the original slow/fast nomenclature is appropriate: Below c^+ the 'fast' (broad) mode has a substantially smaller M_0 than does the 'slow' (sharp) mode. However, the broad mode lifetime of large spheres increases more rapidly with increasing c than does the sharp mode M_0, until for $c \geq c^+$ the M_0 of the two modes become approximately equal. For $c > c^+$ the two modes of large spheres have about the same M_0, but differ in their stretching exponents β. With decreasing probe size, there is a transition from large to small probe behavior. For small 21nm probes the relationship between the modes is reversed: At all concentrations $c < c^+$ the broad mode has the larger M_0. With increasing concentration, the mode lifetimes of these small spheres become more separated; the larger broad mode M_0 increases more rapidly with increasing c than does the smaller sharp mode M_0.

For the smaller 35nm probes in more concentrated polymer solutions, ref. [31] found

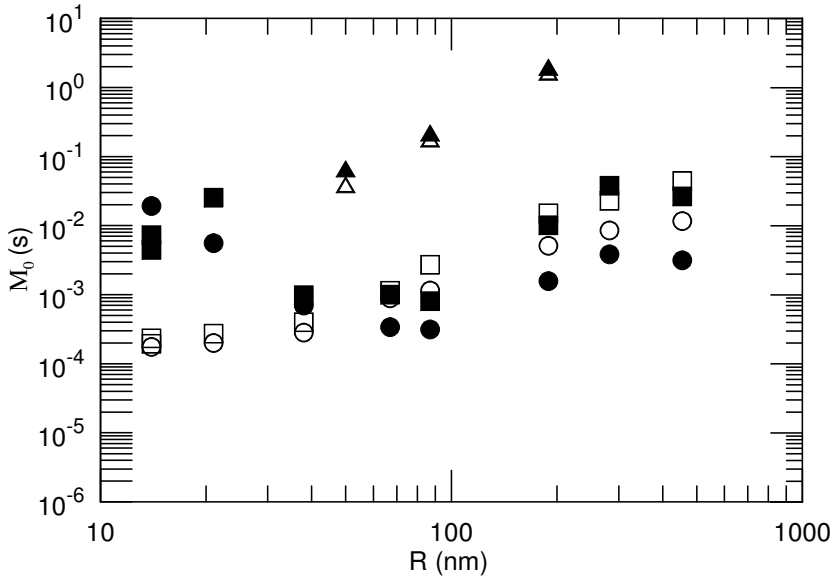

Figure 12: Dependence of the sharp (open points) and broad (filled points) modes of polystyrene latex probes on probe diameter R at concentrations 2 (circles), 4 (squares), and 15(triangles) g/L HPC.

that the probe spectra become trimodal. Figure 11 gives M_0 for the three modes against c. Over $0 \leq c \leq 5$ g/L, the lifetimes M_{0b} and M_{0s} of the broad and sharp modes modes converge, with M_0 of the fastest mode increasing and M_0 the slower mode decreasing until their M_0 are approximately equal. The spectra do not reveal whether above c^+ the two modes remain physically distinct, but happen to have about the same M_0 and different β, or whether the two modes become a single physical relaxation process having a complicated lineshape. In addition to the broad and sharp modes, for $c > c^+$ spectra of 35 nm probes gain an intense, third, 'ultraslow' mode having an extremely long $(0.1 - 10\text{s})$ lifetime. The third mode is extremely broad, with β as small as 0.2 or 0.1 in some solutions.

The dependence of the mode lifetimes on probe diameter appears in Figure 12, which plots M_0 against R for probes in 2, 4, and 15 g/L HPC solutions. For small $(R < 50)$ and large $(R > 180)$ nm probes, M_{0s} of the sharp mode increases approximately linearly with R. Probes of intermediate $(50 \leq R \leq 150)$nm size constitute a transition region in which M_{0s} increases tenfold much more rapidly than linearly in R. The broad mode M_{0b} at first decreases with increasing R and then converges with the sharp mode M_{0s}; above $R \approx 50$nm, M_0 of the sharp and broad modes increase in unison. There is a smallest probe diameter at which $M_{0b} \approx M_{0s}$. While this diameter might have depended on c, we in fact find at each concentration that $M_{0s} \approx M_{0b}$ first is found for ca. 50 nm diameter probes.

As seen in Fig. 13, for large (87, 189nm) probes, the inverse mode lifetimes Γ of the sharp and broad modes are uniformly linear in q^2, the inverse lifetimes going to zero within experimental error in the limit of small q. Small probes present a substantially more complex picture in their q-dependence. For small 20nm probes and $c < c^+$, the sharp mode is the shorter-lived; it is the dominant mode at larger q. As $q \to 0$, the longer-lived broad mode

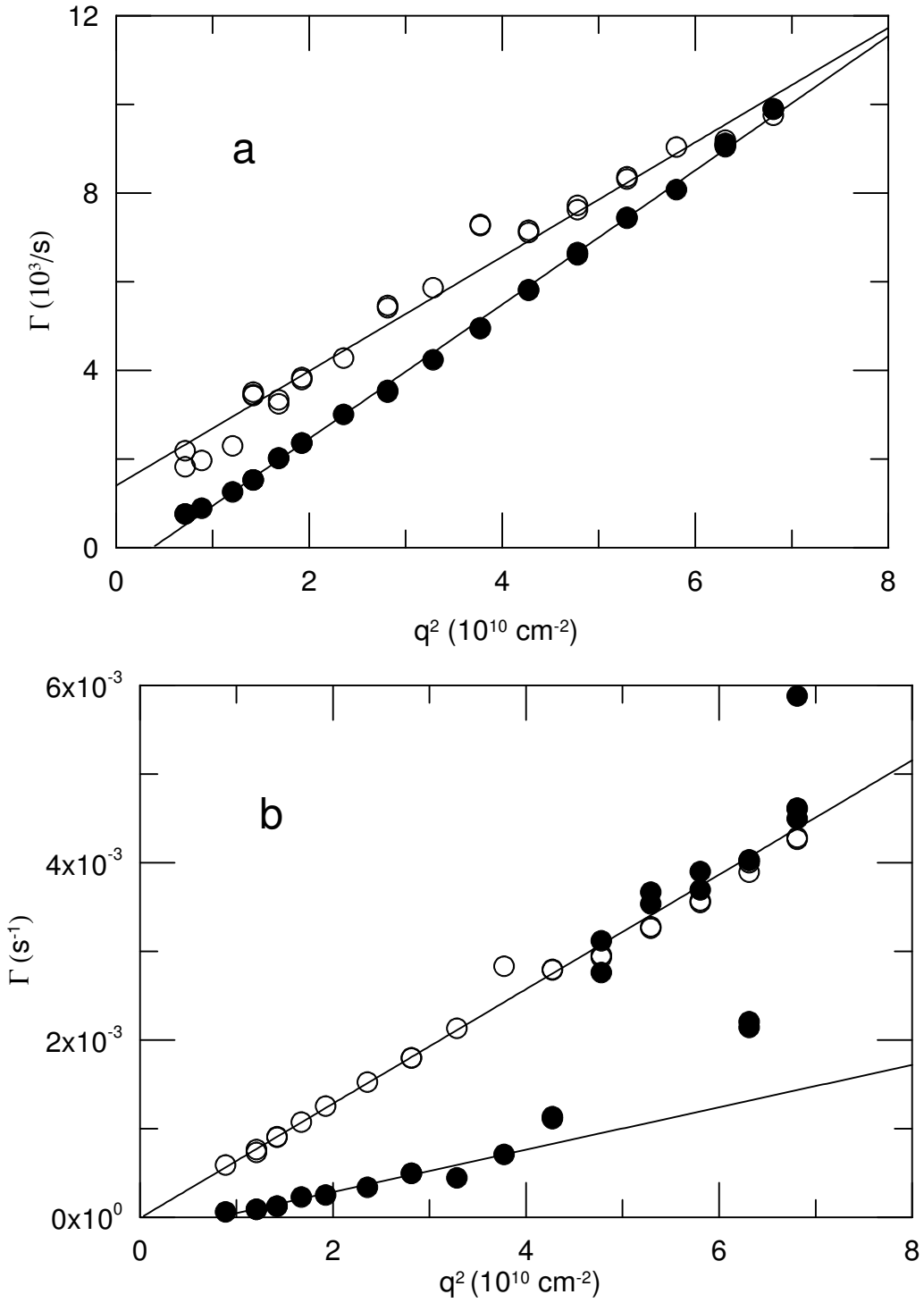

Figure 13: Mean relaxation rates $\Gamma = M_0^{-1}$ for the sharp (open circles) and broad (filled circles) modes of (a) 87 nm probes in 5 g/L HPC and b) 20 nm probes in 4 g/L HPC.

becomes dominant. The sharp mode shows diffusive behavior, with $\Gamma_s \sim q^2$. At small q, Γ_b of the broad mode scales linearly in q^2. Near $q^{-1} \approx 50$nm, Γ_b suddenly increases rapidly. The q^2 dependence of A_s changes markedly near $q^{-1} \approx 70$nm. For large probes, the lineshape parameter β_b and amplitude A_b are both independent of q. In contrast, for small probes and decreasing q, the broad mode tends toward a pure exponential ($\beta_b \rightarrow 1$) and tends toward dominating the spectrum ($A_b \rightarrow 1$) at smaller q.

3.4.5 Temperature Dependence

We[31] examined the temperature dependence of the mode lifetimes, studying 35nm spheres at concentrations $2-15$ g/L at temperatures 6-40 C. While spectra of the 35nm spheres in solutions with elevated polymer concentrations are trimodal, at every concentration there are two dominant modes; namely, the sharp mode is dominant for $c < c^+$, while the ultraslow mode dominates for $c > c^+$. We plotted mean relaxation rates $\Gamma = M_0^{-1}$ against η_o/T, η_o being the viscosity of water at the appropriate temperature. We found that Γ is linear in η_o/T. Γ goes almost to zero as $\eta_o/T \rightarrow 0$. While there are modest intercepts that are not quite zero in the low-temperature limit, the sign of the intercept differs from solution to solution, strongly suggesting that the non-zero intercepts simply reflect noise in the measurements. Above 30 C, a uniform change in M_0^{-1} with increasing T arises from countervailing nonuniform temperature dependences of θ and β. Our results indicate that the observed probe relaxational modes are uniformly controlled by hydrodynamic motions of the solvent, and that nonhydrodynamic processes inherent to the polymer are not affecting probe diffusion substantially.

The temperature dependence of D was also studied by Phillies and Clomenil[24], who used QELSS to examine the diffusion of 67 nm spheres through solutions of 60 kDa HPC in water at temperatures 10 C (good solvent conditions) and 40.5 C (theta solvent conditions). In this early study, spectra were analyzed with a cumulant expansion, which obtains an intensity-weighted average initial slope of $S(q,t)$, and thus obtains a D corresponding to the intensity-weighted average of the visible spectral modes. Polymer concentrations were taken up to nearly 100 g/L, while D at 40.5 C fell from $\approx 1 \cdot 10^{-7}$ down to $\approx 3 \cdot 10^{-10}$ cm^2/s. This early work found that the apparent D fell more slowly with concentration at 10 C than at 40.5 C. When D was fit to a stretched-exponential approximant $D = D_o \exp(-\alpha c^\nu)$, $\nu \approx 3/4$ at 10 C but $\nu \approx 1$ at 40.5 C. This result is not trivially consistent with the observation above that M_0^{-1} depends on temperature as T/η_o at all polymer concentrations. However, as noted above, while M_0^{-1} scaled uniformly with T/η_o, θ and β of each mode did not. D is obtained differently from $S(q,t)$ than M_0^{-1} is; D reflects a different weighting of θ and β; and therefore D may not have the same uniform dependence on T/η_o that M_0^{-1} does. Ref. [24] presented rationales for accepting that the observed temperature dependence of ν is equally consistent with reptation-scaling[63] and hydrodynamic scaling[4, 64] models of polymer dynamics.

3.4.6 Molecular Weight Dependence

In addition to the early work of Yang and Jamieson[52], studies revealing the molecular weight effects on probe diffusion have appeared from this laboratory[23, 27]. Ref. [23] examined intermediate-size 67nm probes in solutions of 139, 146, 415, and 1280 kDa HPC

at three temperatures, reaching viscosities up to $10^3 - 10^6$ cP. Cumulant expansions were used to extract the initial logarithmic derivative (and hence the z-average diffusion coefficient D) from the spectra, which were obtained over a narrower time range than used by Streletzky's studies described above. Fits to a single stretched exponential ($\exp(-\theta t^\beta)$ or $\exp(-(t/\tau)^{-\beta})$) in time were used to provide an alternative parameterization of the same spectra. D and τ are both described accurately by stretched exponentials $\exp(-\alpha c^\nu)$ in polymer concentration. To describe τ, the magnitude of α increases four-fold (at 10 C) or seven-fold (at 39 C) as M increases from 139 to 1280 kDa. The concentration dependences of D and τ are not explained by the concentration dependences of the solution viscosities. The products $D\eta$ and τ/η deviate from unity as progressively-increasing stretched exponentials in c. The deviations are smallest (less than a factor of 3) for solutions of the 138 kDa HPC, and largest (up to 100-fold) for solutions of the 1280 kDa HPC. There was absolutely no indication of a return to Stokes-Einsteinian behavior (i.e., $D\eta$ did not fall back toward its zero-concentration value) at elevated polymer concentration, even though solutions were under transient lattice theories very substantially entangled, with η up to 10^6 for the largest-M polymers.

Phillies and Lacroix[27] report on diffusion of 21, 109, 189, and 760nm diameter polystyrene latex spheres as optical probes in aqueous 415kDa HPC at polymer concentrations up to 15 g/L, corresponding to solution viscosities up to 100 times the viscosity of water. They found that their probe spectra were described accurately by a stretched exponential $\exp(-\theta t^\beta) \equiv \exp(-(t/\tau)^\beta)$ in time, with a superposed weak pure exponential at early times. Figure 13 shows the relaxation pseudorate θ and scaling exponent β for the four probes. From Figure 13a, over the observed range of concentrations θ for the large spheres changes by a hundred-fold, but θ for the small spheres changes by no more than ten-fold. Over the same concentration range, from Figure 13b β falls from very close to unity for probes in pure water to 0.8 or 0.9 for probes in 15 g/L 415 kDa HPC. On comparison with β for probes in 1MDa HPC, we infer that the observed relaxational mode is a sharp mode (β close to 1) rather than a broad mode (β around 0.5).

It would alternatively be possible to parameterize $S(q,t)$ as a function of τ rather than θ. By comparing the concentration dependences of θ and τ with the concentration dependence of the viscosity η, we can make inferences as to whether θ or τ is more fundamental from a physical standpoint. Figure 15 plots $\theta\eta$ and τ/η against c. For the small probe, $\theta\eta$ climbs almost ten-fold with increasing c. With increasing probe diameter, the dependence on c of $\theta\eta$ becomes less and less, until for the 760nm probes $\theta\eta$ is substantially independent of polymer concentration. We infer that precisely the same issues govern the concentration dependences of η and of θ of these very large probes. In contrast, from Figure 15 τ/η depends at least weakly on polymer concentration even for 760nm spheres. If one expected that diffusion of extremely large probes should be governed by the measured macroscopic viscosity, then one would conclude that θ rather than τ offers a fundamental description of probe motion.

Probes diffusing in simple liquids have spectra characterized by $g^{(1)}(q,t) \sim \exp(-Dq^2t)$ and $D \sim \eta^{-1}$, i.e., exponentially decaying spectra with diffusion coefficients showing Stokes-Einsteinian behavior. The spectra here are stretched, not simple, exponentials in time. Correspondingly, while θ and Dq^2 both characterize the spectral relaxation, they do not have the same dimensions, so it would be improper to identify θ as a Dq^2. Similarly,

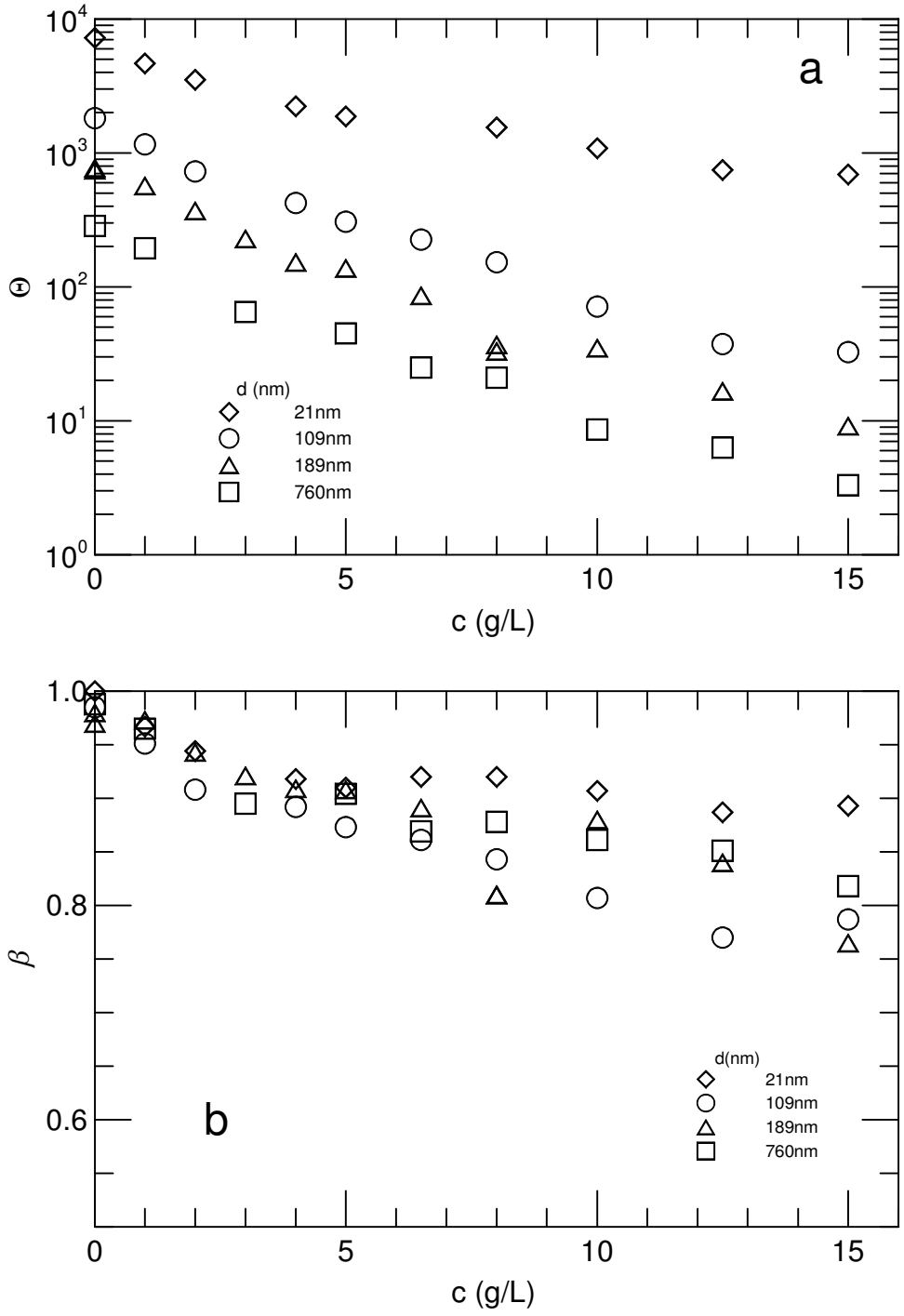

Figure 14: (a) θ and (b) β as functions of polymer concentration for probe spectra of spheres in 415 kDa HPC:water.

even though $\theta \sim \eta^{-1}$ looks rather like $Dq^2 \sim \eta^{-1}$, θ is not a diffusion coefficient, and correspondingly $\theta \sim \eta^{-1}$ cannot be said to be Stokes-Einsteinian behavior. The relationship between θ and η for all but the largest spheres indicates that η cannot be the only physical parameter, whose dimensions include time to a non-zero power, that contributes to θ.

3.4.7 Smaller and Small-Chain Probes

Probe diffusion by truly small probes was observed by Mustafa, et al.[32] and Bu and Russo[33], who used fluorescence recovery after photobleaching to observe diffusion by fluorescein[32, 33] and dye-tagged dextrans[33] through HPC solutions. FRAP is only sensitive to extremely large molecular displacements, which take much time to transpire, so the multimodal structure observed with QELSS is not apparent in FRAP spectra. They observe single-exponential spectra $\exp(-\Gamma t)$ whose decay rates Γ are quadratic in the photobleach grating wavelength. Mustafa, et al.[32] observed diffusion through solutions of $M_w \approx 130$ kDa, 292 kDa, and 855 kDa HPC, at HPC weight fractions extending from zero up to 0.58. D of the fluorescein declines as a simple exponential $\exp(-\alpha c^1)$ in HPC concentration, with the exponential prefactor α being independent of polymer molecular weight over more than a six-fold variation in M_w. Mustafa, et al.[32] report that the concentration dependence of D is considerably larger for dye molecules in HPC solutions than for dyes in solutions of organophilic polymers in organic solvents. They also report that the temperature and concentration dependences of D show 'no pronounced discontinuities...as the lyotropic liquid crystal boundary is crossed." Mustafa, et al.'s data is consistent with the plausible interpretation that dye diffusion involves interaction with local segment dynamics, but that whole chain motion is not an active component of the process that permit dye molecules to diffuse, albeit slowly, through HPC solutions.

Bu and Russo[33] report on fluorescein, dextrans with eight molecular weights $3.9 \leq M_w \leq 2000$kDa, and 55nm diameter polystyrene latex spheres diffusing through solutions of 300 kDa HPC at HPC weight fractions from 0 to 0.039. Solution viscosities were also measured. D was found to follow the Langevin-Rondelez[63] equation

$$D/D_o = \eta_o/\eta + \exp(-(R_h/\xi)^\delta) \tag{25}$$

In this form, D_o and η_o are the probe diffusion coefficient and viscosity for the pure solvent, R is a radius for the probe particles, ξ is a hypothesized solution length scale determined by polymer concentration but not polymer molecular weight, and δ is a scaling exponent. In the analysis ξ was obtained from fits to the data at each concentration, finding $\xi \approx 10$nm at 10 g/L HPC and $\xi \approx 3$nm at 39 g/L HPC.

Bu and Russo report the dependence of D on probe molecular weight (and, hence, probe radius) for dye and eight labelled dextrans in solutions of 300 kDa HPC. Their outcomes are qualitatively very similar to those in Figures 7 and 13. For smaller probes, D depends only weakly on polymer concentration. For larger probes, the dependence of D on HPC concentration is quite marked, and increases appreciably as the probe M is increased. The transition from small- to large probe behavior occurs for probes with $M_w \geq 18.9$ kDa, perhaps ≥ 40.5 kDa, corresponding to probe hydrodynamic diameters 3.4–5.6 nm. For 300 kDa HPC, interpolation of the results of Yang and Jamieson[52] suggests an R_h for the HPC of approximately 30nm, so the small- to large-probe transition seen by Bu and Russo

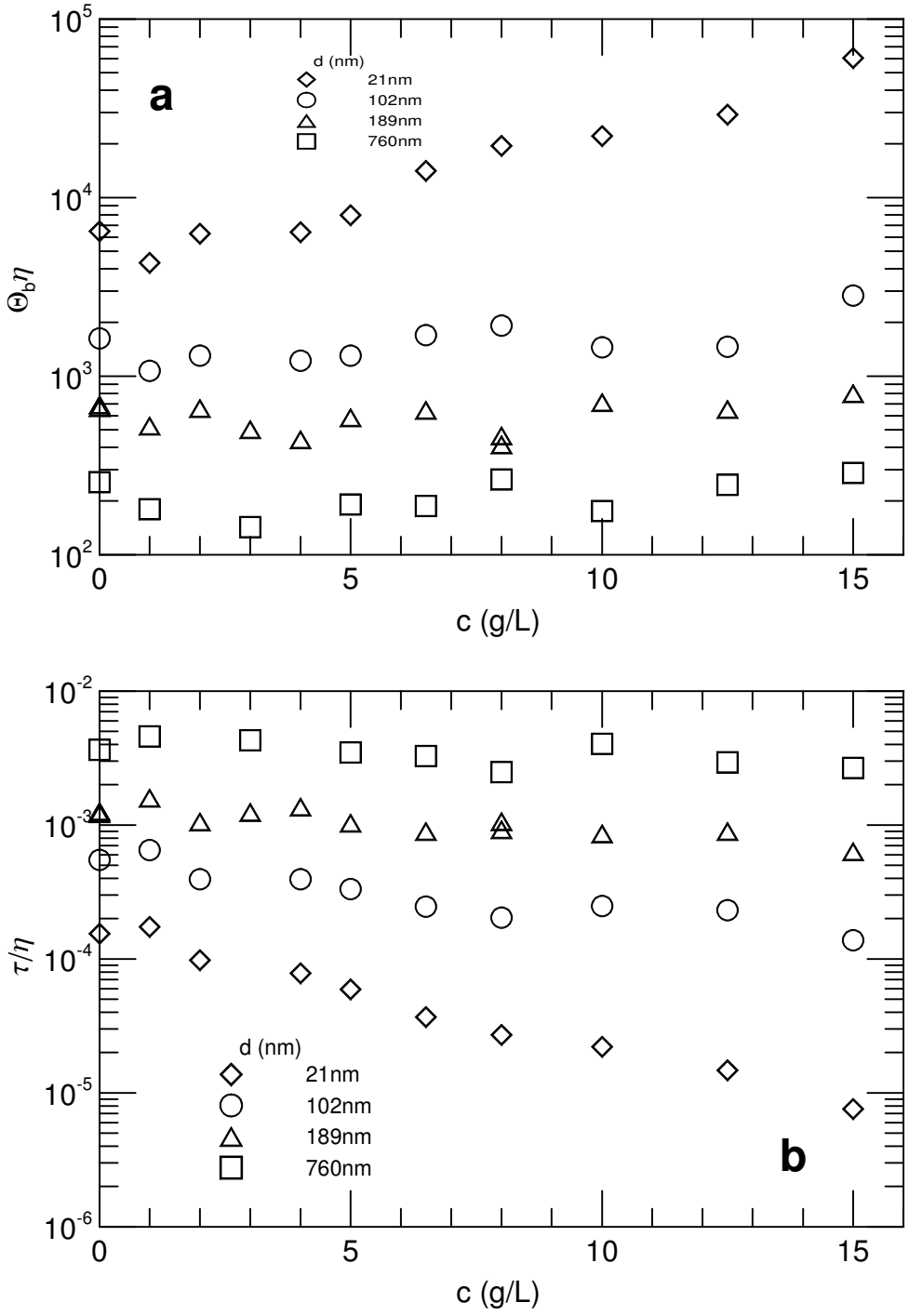

Figure 15: Relation between decay pseudorate and pseudotime and solution viscosity, for probes in HPC: water[27], namely a) $\theta_s\eta$ and b) τ/η against c.

occurs for probes that are substantially smaller than the matrix polymer chains. However, Bu and Russo's probes are random-coil polymers, not hard spheres, so their outermost segments are remote from the center of mass by appreciably more than their R_h or R_g. The radius R_g of the dextrans, which was not reported by Bu and Russo, is perhaps twice the R_h. Furthermore, R_g of a hard sphere is 3/5 of the sphere radius r, so a dextran with $2R_h \approx 4$ nm has approximately the same $2R_g$ as a $2r \approx 13$nm hard sphere. The solution length scale ξ implied by the probe behavior observed by Bu and Russo is therefore a reasonable fraction of the size of a polymer chain.

The probes in question are semirigid dextrans, not space-filling polystyrene latex spheres. In their Figure 4, Bu and Russo[33] plot the apparent solution microviscosity as a function of probe size, for probes extending from the $R_h = 0.05$ nm fluorescein dye through eight dextrans (1.32-17.9 nm) up to 55.1 nm polystyrene spheres. η_μ increases smoothly with increasing probe size, but is never as large as the macroscopic viscosity η. At fixed polymer concentration, η_μ for random-coil dextrans and for hard spheres (polystyrene latex, dye molecules) depend on probe size via a single smooth curve, without substantial differences between η_μ of dextran chains and spherical probes other than those attendant to their sizes.

4 Comparison with Ngai-Rendell Coupling Model

We compared our experimental results with predictions of the Ngai-Rendell coupling model[34, 35], which has been successfully applied to a variety of chaotic and strongly interacting complex systems [36, 37, 38, 39] including polymer solutions [34, 60, 61]. The Ngai-Rendell model focuses on apparently-universal features of the cooperative dynamics of complex systems, proposing that these features arise from the systems' dynamic constraints.

The model treats complex systems as collections of nonlinearly-interacting basic units. At times shorter than t_c, the basic units relax independently, with relaxations described by a pure-exponential time correlation function $\phi(t) \sim \exp(-t/\tau_0)$. Here τ_0 is the characteristic time for unconstrained relaxation. At times t longer than t_c, cooperative constraints between the units govern relaxations. As a result, relaxations have stretched-exponential time correlation functions $\phi(t) \sim \exp(-(t/\tau)^{1-n})$. The stretching exponent $1-n$ is determined by the degree of coupling $n \leq 1$ between basic units, while τ is the characteristic time for constrained relaxation. In polymer solutions the dynamic constraints are the interactions between chains that control the relaxation rates. The coupling model does not specify which interactions (e.g. hydrodynamic or topological) create the dynamic constraints; it only specifies that the constraints exist. The coupling model is equally applicable to nondilute polymer systems and to mesoscopic probes in polymer solutions.

Several important predictions of the Ngai-Rendell model are consistent with the phenomenology of probe and polymer diffusion. First, the stretched-exponential lineshape $g^{(1)}(t)$ of the field correlation function obtained from light scattering $\phi(t)$ is indeed a stretched exponential with stretching exponent $\beta_t \sim 1-n$. Second, the coupling model is consistent with the observed stretched-exponential concentration and molecular weight dependences observed in many systems for η and D_s. Third, the coupling model predicts a dependence of $\beta \equiv 1-n$ on c that is consistent with $\beta(c)$ in many polymer systems[34, 60, 61].

Fourth, the coupling model predicts that the relaxation time $\tau = \theta^{-1/\beta}$ of eq. 12 follows $\tau \sim q^{-2/\beta}$ as seen in several polymer solutions.

In addition, for non-dilute solutions Ngai and Phillies[26] extended the coupling model to connect the parameter n_d to the concentration dependence of D from eq. 23, namely

$$\beta_c \equiv 1 - n_d = [\frac{3\nu}{2} + \frac{(3\nu - 1)(\ln(D_s(c^*)) - \ln(D_s(c)))}{2\ln(c/c^*)}]^{-1}. \quad (26)$$

Here c^* is a nominal overlap concentration, and ν relates polymer radius of gyration R_g and its molecular weight M via $R_g \sim M^\nu$. For the case when θ was approximately $\sim \eta^{-1}$ and $\sim q^2$, Ngai and Phillies [26] argued for replacement of D_s with θ in eq. 26.

Ref. [26] also develops coupling/scaling arguments to obtain coupling parameters β_η and n_η from the concentration dependence of η, namely

$$\beta_\eta \equiv 1 - n_\eta = [\frac{3\nu}{2} + \frac{(3\nu - 1)(\ln(\eta(c)) - \ln(\eta(c^*)))}{2\ln(c/c^*)}]^{-1}. \quad (27)$$

The derivation of β_η uses coupling/ scaling analysis without any auxiliary assumptions.

Equations 11, 26, and 27, and the q-dependence of θ provide four independent ways to obtain the coupling parameter n: i) from the time dependence of $g^{(1)}(t)$, ii) from the concentration dependence of θ, iii) from the concentration dependence of η, and iv) from the angular dependence of τ in $g^{(1)}(t)$. Ngai and Phillies [26] used the first three paths to obtain n from experimental data on probes in 415kDa HPC [27]. The n calculated from the time dependence of $g^{(1)}(t)$ and from the concentration dependences of θ and η all agree with each other, supporting the validity of the coupling-scaling *ansatz* as a useful frame for treating polymer solution dynamics. Applying the coupling model in this case was unambiguous because Ref. [27] reported spectra with a single stretched-exponential relaxation.

Probe diffusion experiments in 1MDa HPC[30] revealed not one but two relaxational modes. Therefore, applying the analysis of Ref. [26] to this data was impossible. The broad and sharp modes appear to have different physical natures. One interpretation of the bimodal structure is that the system contains two independent groups of basic units, strongly coupled within each group, but weakly coupled between groups. Physically, these basic units might represent different chain modes of motion, such as center-of-mass motion and rotation. We applied the coupling/scaling model separately to each mode to see when model predictions are followed. From eqs 11 and 26 we obtained two sets of coupling coefficients: β_{tb} and β_{cb} for the broad mode and β_{ts} and β_{cs} for the sharp mode. These coefficients were all compared with β_η, which reflects a solution property measured in the absence of probe particles.

In solutions of 1 MDa HPC, some modes follow coupling-scaling predictions; others do not. The broad mode of small probes has a tolerable agreement with the coupling model, while the sharp mode of large probes is very successfully described by coupling/scaling. The broad mode of large probes and the sharp mode of small probes do not follow these predictions. For small probes, the broad mode is dominant, and coupling/scaling is applicable to the dominant mode. However, for large probes the two modes have roughly the same amplitude though very different θ, and coupling/scaling only applies to one of them. Regardless of the probe size, one can distinguish a shorter and a longer-lived mode. For small probes, the shorter-lived mode is the broad mode, while for large probes the shorter-lived

mode is the sharp mode. Both shorter-lived modes thus follow coupling/scaling predictions, but both longer-lived modes (the small-probe broad mode and the large-probe sharp mode) do not. The Ngai-Rendell coupling model succeeds on short and intermediate but not long time scales.

Recently, we made additional experiments on probes in 415kDa HPC, using a newer and more sensitive spectrometer[68]. We found a weak sharp mode for small probes and a weak broad mode for large probes. The newly-observed sharp mode of small probes and broad mode of large probes are the longer-lived modes, while the modes (small-probe sharp mode, large-probe broad mode) that were previously observed and that follow the Ngai-Rendell model predictions are the shorter-lived modes. Spectra of probes in 415kDa HPC agree with probe spectra in 1MDa HPC.

5 Conclusions

Systematic studies of light scattering spectra and other static and dynamic solution properties of aqueous hydroxypropylcellulose solutions lead to a coherent image of the dynamics of this semirigid neutral polymer. In particular

- Diffusive modes of optical probe motion through polymer solutions differ substantially from diffusive modes for the polymer chains on the same distance scale.
- The solutionlike-meltlike transition is equally apparent in the concentration dependences of the shear viscosity, light scattering spectra of polymer solutions, and optical probe spectra, but has no consequence for the static scattering intensity.
- The dynamics of aqueous hydroxypropylcellulose are characterized by a single length scale $\approx$ 50-70nm that does not depend strongly on concentration.
- The correlation between the probe diffusion rate (however parameterized) and the solution viscosity is determined by the ratio of the probe and chain radii.
- Having in past work characterized probe spectra with decay pseudorates θ or pseudotimes τ, we conclude that the spectral time moment M_0 substantially clarifies our observations.

Some aspects of this image are not transparently consistent with some models for polymer dynamics. In particular, the primary length scale is roughly the size of a polymer chain, not the distance between two of the hypothesized entanglement points; nor does the observed length scale depend strongly on concentration. Our results do however lead to a plausible model for our observations, namely that at the solutionlike-meltlike transition marks the formation of a generalized Kivelson[65] glass.

We now consider these points in more detail.

First, *diffusive modes of optical probe motion through polymer solutions are not simply the diffusive modes of the polymer chains on the same distance scale.* The probe spheres and the polymer chains do not simply move in unison with each other. Some probes have mode lifetimes that are not very different from the mode lifetimes of the polymers through

which they are diffusing. However, while the lifetimes are not very different, the concentration dependences differ appreciably: The M_0 of the fast and intermediate polymer modes *decrease* as the polymer concentration is increased. The M_0 of the fast and intermediate probe modes depend on the probe size, but generally *increase* with increasing polymer concentration. (However, the slow mode of the polymer solution, seen only for $c > c^+$, occurs on about the same time scale as the slow mode of the 35 nm probe spheres, which is also seen only for $c > c^+$.)

Second, *the solutionlike-meltlike transition is equally apparent in the concentration dependences of the shear viscosity, light scattering spectra of polymer solutions, and optical probe spectra, but has no consequence for the static scattering intensity.* For the shear viscosity, at the transition η unambiguously goes over from a stretched-exponential concentration dependence to a power-law concentration dependence at concentration c^+[25]. Streletzky and Phillies[29, 64, 66] studied scattering from large ($R > 50$ nm) polystyrene sphere probes in the solutionlike and meltlike regimes, using lineshape parameters θ and β. They found that the concentration dependences of θ_b, β_b, $d(\theta_b\eta)/dc$, and the broad mode amplitude A_b all change markedly at a concentration near c^+. In particular, below c^+, A_b increases markedly with increasing c, but at higher concentrations is nearly independent of c. β_b falls with increasing c until c^+ is reached and then becomes constant or increases slowly. Above c^+, θ_b decreases with increasing c; below c^+, θ_b increases with increasing c. Phillies, et al.[31] studied small 35 nm probes above and below c^+, computing M_0 for each mode of these probes and comparing with M_0 for other probes. The scattering spectra of these small probes have an ultraslow mode, but only at concentrations above c^+. For large probes, M_0 of the sharp and broad modes become equal for c greater than approximately 4 g/L. O'Connell, et al.[59], studying light scattering spectra of 1 MDa HPC: water, found that HPC itself gains a new ultraslow spectral mode at concentrations above 6 g/L or so, this being the concentration c^+. The sudden appearance of the slow spectral mode was not accompanied by a sudden increase in the intensity of the scattered light.

The solutionlike-meltlike transition is apparent in the shear viscosity, in optical probe spectra of probes having a wide range of sizes, and in light scattering spectra of the HPC solutions themselves. We conclude that it is a real physical effect. Furthermore, because the viscosity transition and the neutral polymer slow mode are each seen only with some high-molecular weight polymers and not others[67], it cannot be the case that the solutionlike-meltlike transition corresponds to a universal property of polymers arising, e.g., from their topology and chain non-crossing constraints.

Third, *the dynamics of 1 MDa aqueous hydroxypropylcellulose are characterized by a single length scale* $\xi \approx$ 50-70*nm that does not depend strongly on concentration.* The same physical length reasserts itself at a long series of points in our measurements, and no other length scale is evident, leading us to identify ξ as *the* characteristic length scale for our polymer solutions.

Circumstances in which the length scale asserts itself include: (i) (Figure 7a) Below c^+, for small probes (diameters $R < \xi$), θ_s is nearly independent of c; for large probes (diameters $R > \xi$), θ_s depends markedly on c. (ii) (Figure 7b) Below c^+, for small probes, the range of θ_b values is nearly independent from R; for larger probes, θ_b falls markedly with increasing R. (iii) (Figure 6a) $\beta_s \approx 1$ for large probes but β_s falls with increasing c for small probes. (iv) (Figure 12) Above c^+, small probes show an ultraslow mode; large

probes do not. (v) Below c^+, for small probes M_0 of the broad mode is larger than M_0 of the sharp mode; for large probes, the broad mode is shorter-lived (smaller M_0) than the sharp mode[31]. (vi) For small probes, the sharp mode dominates at large q while at small q the longer-lived broad mode is dominant; the crossover distance is $q^{-1} \approx 70$ nm[31]. (vii) (Figure13b) The relaxation rate M_0^{-1} of 20 nm probes in 4 g/L HPC has a dramatic transition near $q^{-1} \approx 50$ nm. (viii) The concentration dependence of the longer-lived probe mode increases substantially when the mode becomes longer-lived than the HPC intermediate mode. Depending on the probe diameter, this increase occurs at different polymer concentrations[31]. For a particular probe, namely the 50nm probes, the increase occurs near the rheologically-interesting concentration c^+.

In each of these cases, the same distance demarks different domains of behavior. For 1 MDa HPC, 50 nm is close to the polymer hydrodynamic radius R_h [52]. That is, the characteristic length that is important for the diameter of these polymers is a length that characterizes the chain size, not the distance between pairs of interchain contacts. From Figure 7, ξ remains near 50 nm over a 15-fold range of concentration that extends from dilute solutions through semidilute solutions ($c > 4[\eta]$) and into the meltlike regime $c \geq c^+$. ξ might depend weakly on c. The data reject a form $\xi \sim c^{-\nu}$ for a ν of 0.5 or 1.0.

Fourth, *the correlation between the probe diffusion rate (however parameterized) and the solution viscosity is determined by the ratio R_p/R_c of the probe and chain radii.* The study of Bu and Russo[33] using probes with diameters from a few Angstroms to 55 nm, and Lacroix and Phillies[27] and Streletzky and collaborators[28, 29, 30, 31] using a wide range of probes and polymer chains are entirely consistent with each other. Experimentally, η_μ/η is almost always less than unity. The smaller the probe, the smaller is η_μ/η. The diffusion rate only tracks η if $R_p/R_c \gg 1$. η_μ/η always falls progressively with increasing polymer molecular weight M, because increasing M while leaving the probe unchanged reduces the ratio R_p/R_c. η_μ/η also always falls with increasing c. Models that predict that the important polymer length scale is the distance ξ_c between polymer entanglement points, and not the size of the chain as proposed here, are not compatible with this result: Increasing c increases R_p/ξ_c and thus according to these models would move η_μ/η toward unity, in contradiction to almost all experiment.

Fifth, *having in prior work characterized probe spectra with decay pseudorates θ or pseudotimes τ, we conclude that the spectral time moment M_0 substantially clarifies our observations.* In particular, Ngai and Phillies[26] and Streletzky and Phillies[30] compared θ and β from optical probe data and the viscosity with predictions of the Ngai[34] coupling-scaling model. The Ngai model was found to explain the concentration dependence of the sharp mode of small probes and the broad mode of large probes, but did not explain the behavior of the small-probe broad mode or the large-probe sharp mode. It seemed difficult to explain why the model should work for one mode of some probes, and the other mode of other probes. However, the identity of the longer-lived of the broad and sharp modes alternates between small and large probes. For all probes, the Ngai coupling-scaling model describes the behavior of the shorter-lived of the sharp and broad modes. Describing mode lifetimes with M_0 thus unifies the data, showing that the Ngai mode is good at short and intermediate times, but there are complications at really long times.

Furthermore, an examination of the mode amplitudes at small q shows that: For large probes, the sharp mode is dominant at all q. For small probes, as $q \to 0$ the broad mode

becomes dominant, with fractional amplitude ≈ 1 at small q. It seemed difficult to understand why different modes should dominate at small q for different probes. However, the large-probe sharp mode and the small-probe broad mode are both the longer-lived of the two modes. It is entirely reasonable that for diffusion over large distances the longer-lived of the two modes should be dominant in the dynamics. Diffusion over long distances takes a long time, so it is plausible that short-lived relaxations will decay far before the probe has moved a large distance.

Contrariwise, for small probes at long times the broad mode is the longer-lived. Therefore, the small-probe diffusive process does not lead to simple diffusion at long times, the simple Langevin equation does not describe probe motion even at long times, and the mean-square particle displacement is not linear in elapsed time even at long times. It is then meaningless to construct a D from $\langle(\Delta x)^2\rangle/\Delta t$. Non-Langevin diffusion processes at long times might not arise if the system had a single well-defined longest length scale, but might arise if chain dynamics had interesting long-range interactions, which they are known to have.

Finally, *the solutionlike-meltlike transition has properties consistent with a transition from a liquid toward a generalized Kivelson[65] glass.* We say *generalized* Kivelson glass because the system here differs in minor ways from that envisioned by Kivelson, et al., in particular the 'atomic' objects are polymer chains rather than simple spheres, and the system is a (relatively) athermal solution rather than a simple fluid, so concentration rather than temperature is the primary thermodynamic control variable. In the original model as proposed by Kivelson, glass formation was proposed to arise from the formation of growth-limited frustrated molecular clusters. The hypothesized clusters were not crystallites of the stable phase. Instead, they were clusters whose repeat structure is not space-filling, so they cannot grow to fill all space. The clusters enhance viscosity by enhancing molecular jamming at low temperatures. Because the clusters are not crystallites, they can have a distinct melting temperature that can be higher than the melting temperature of the crystal. Such high-melting static clusters have recently been seen in molecular dynamics simulations by Whitford and Phillies[69].

Here the concentration is the control variable. Low concentrations are analogous to high temperatures, and vice versa; at high temperatures or at low concentrations clusters do not form. Clusters form when the temperature is reduced or correspondingly when the concentration is increased. By direct analogy with Kivelson's original clusters being stable below some temperature T_m (that is appreciably warmer than the crystal-phase melting temperature, as observed simulationally[69]), growth-limited solution clusters are stable above some concentration c_c that is less than the solubility limit concentration. We identify c_c with the solutionlike-meltlike transition concentration c^+. Our data support the interpretation that c^+ corresponds to cluster formation, namely: (i) The clusters first appear at a well-defined concentration and increase smoothly at larger concentrations, leading the phenomena that set in at a well-defined concentration c^+. (ii) Probes smaller than a cluster could be entrained by that cluster, and would diffuse at the same rate as the cluster. Indeed, small but not large probes exhibit the ultraslow mode that appears at the onset of cluster formation. (iii) At c^+, the ultraslow mode appears discontinuously; an ultraslow mode is a plausible concomitant of clusters.

Light scattering measurements provide some information on the nature of the clusters. I/c shows no discontinuity as one passes from below to above c^+, indicating that the clusters cannot have an internal concentration that is significantly different from that of the bulk solution: If the internal and bulk concentrations differed significantly cluster formation would lead to substantially enhanced static light scattering by the solutions. The high-melting static clusters observed by Whitford and Phillies[69] have precisely this same property, namely the internal density of a cluster does not differ from the density of the bulk fluid. Furthermore, our studies of temperature dependence find that the mean relaxation times depend on temperature as η_o/T, η_o being the temperature-dependent solvent viscosity, so the dynamic process seen here are controlled by solvent motion (hydrodynamics), not by internal rate processes that do not involve the solvent.

Acknowledgements

The authors would like to acknowledge and express gratitude to M. LaCroix, H. Hanson, R. O'Connell, C. Richardson, C. Quinlan, and J. Yambert for research collaborations. Portions of this work were supported by the National Science Foundation under several grants.

References

[1] Graessley, W. W. Adv. Polymer Sci. 1974, 16, 1-179.

[2] McLeish, T. C. B. Adv. Physics 2002, 51, 1379-1527.

[3] Doi, M.; Edwards, S. F. The Theory of Polymer Dynamics, Clarendon Press: Oxford, UK, 1986.

[4] Phillies, G. D. J. Macromolecules 1987, 20, 558-564.

[5] Phillies, G. D. J. J. Phys. Chem 1989, 93, 5029-5039.

[6] Skolnick, J.; Kolinski, A. Adv. Chem. Phys. 1990, 78, 223-278.

[7] Baumgartner, A.; Muthukumar, M. Adv. Chem. Phys. 1996, 94, 686.

[8] Lodge, T. P.; Rotstein, N.; Prager, S. Adv. Chem. Phys. 1990, 79, 1-132.

[9] Werbowyj, R. S.; Gray, D. G. Macromolecules 1980, 13, 69-73.

[10] Guido, S. Macromolecules 1995, 28, 4530-4539.

[11] Larez-V, C.; Crescenzi, V. Ciferri, A. Macromolecules, 1995, 28, 5280-5284.

[12] Grizzuti, N. Maffettone, P. L. J. Chem. Phys. 2003, 118, 5195-5200.

[13] Takebe, T.; Hashimoto, T.; Ernst, B.; Navard, P. J. Chem. Phys. 1990, 92, 1386-1396.

[14] Godinho, M. N.; van der Klink, J. J.; Martins, A. F. J. Phys. Condensed Matter 2003, 15, 5461-5468.

[15] Zhang, Y.; Tun, Z.; Ritcey, A. M. Langmuir 2004, 20, 6187-6194.

[16] Sebastiao, P. J.; Crus, C.; Pires, D.; Ferraz, A.; Brogueira, P.; Godinho, M. N. Liquid Crystals 2002, 29, 1491-1495.

[17] Lee, K.; Lawandy, N. Optics Communications 2002, 203, 169-174.

[18] Brydon, G.; Ganguly, R.; Ghosh, S. GUT Apr 2003 Supplement 1, 52, pA9.

[19] Watano, S. et. al., Powder Technology, 2004, 141, 172-176.

[20] Francis, M.; Piredda, M.; Winnik, F. J. Controlled Release 2003, 93, 59-68.

[21] Xia, X.; Tang, S.; Lu, X.; Hu, Z. Macromolecules 2003, 36, 3695-3698.

[22] Sinha Roy, D.; Rohera, B. Eur. J. Pharmaceutical Sci. 2002, 16, 193-199.

[23] Phillies, G. D. J.; Richardson, C.; Quinlan, C. A.; Ren, S. Z. Macromolecules 1993, 26, 6849-6858.

[24] Phillies, G. D. J.; Clomenil, D. Macromolecules 1993, 26, 167-170.

[25] Phillies, G. D. J.; Quinlan, C. A. Macromolecules 1995, 28, 160-164.

[26] Ngai, K. L.; Phillies, G. D. J. J Chem. Phys. 1996, 105, 8385-8397.

[27] Phillies, G. D. J.; LaCroix, M. J. Phys. Chem **B** 1997, 101, 39-47.

[28] Streletzky, K. A.; Phillies, G. D. J. J. Chem. Phys. 1998, 108, 2975-2988.

[29] Streletzky, K. A.; Phillies, G. D. J. Macromolecules 1999, 32, 145-152.

[30] Streletzky, K. A.; Phillies, G. D. J. J. Phys. Chem. **B** 1999, 103, 1811-1820.

[31] Phillies, G. D. J.; O'Connell, R.; Whitford, P.; Streletzky, K. A. J. Chem. Phys. 2003, 119, 9903-9913.

[32] Mustafa, M. B.; Tipton, D. L.; Barkley, M. D.; Russo, P.S.; Blum, F. D. Macromolecules 1993, 26, 370-378.

[33] Bu, Z.; Russo, P.S. Macromolecules 1994, 27, 1187-1194.

[34] Ngai, K. L. in *Disorder Effects in Relaxation Processes*, Richert, R.; Blumen, A., Eds.; Springer, Berlin, Berlin, 1994, pp. 89-150.

[35] Tsang, K. Y.; Ngai, K. L. Phys. Rev. E 1996, 54, R3067-R3070.

[36] Ngai, K. L.; Plazek, D. J.; Rendell, R. W. Rheologica Acta 1997, 36, 307-319.

[37] Ngai, K. L.; Tsang, K. Y. Macromol. Symp. 1995, 90, 95-129.

[38] Ngai, K. L.; Rajagopal, A. K.; Lodge, T. P. J. Polym. Sci. Polym. Physics 1990, 28, 1367-1377.

[39] Rendell, R. W.; Ngai, K. L.; McKenna, G. B. Macromolecules 1987, 20, 2250-2256.

[40] Kivelson, D.; Tarjus, G. J. Chem. Phys. 1998, 109, 5481-5486.

[41] Swensen, H. A.; Schmitt, C. A.; Thomson, N. S. J. Polym. Sci., Part C 1965, 11, 243.

[42] Kamide, K.; Saito, M.; Suzuki, H. Makromol. Chem. Rapid Communications 1983, 4, 33.

[43] Aharoni, S. M. Macromolecules 1983, 16, 1722-1728.

[44] Phillies, G. D. J. J. Chem. Phys. 1974, 60, 976-982.

[45] Phillies, G. D. J. J. Chem. Phys. 1974, 60, 983-989.

[46] Phillies, G. D. J. Biopolymers 1975, 14, 499-508.

[47] Turner, D. N.; Hallett, F. R. Biochim. Biophys. Acta 1976, 451, 305-312; Russo, P. S.; Mustafa, M.; Cao, T.; Stephens, L. K. J. Colloid Interface Sci. 198, 122, 120-137; Brown, W.; Rymden, R. Macromolecules 1986, 19, 2942-2952; Furukawa, R.; Arauz-Lara, J. L.; Ware, B. R. Macromoelcules 1991, 24 599-605.

[48] Berne, B. J.; Pecora, R. Dynamic Light Scattering; John Wiley and Sons: New York, NY, 1976, especially Chapter 5.

[49] Altenberger, A. R.; Deutch, J. M. J. Chem. Phys. 1973, 59, 894-898.

[50] Doob, J. L. Annals Math. 1942, 43, 319-369.

[51] Russo, P. S.; Mustafa, M.; Cao, T.; Stephens, L. K. J Colloid Interface Sci. 1988, 122, 120-137.

[52] Yang, T.; Jamieson, A. M. J. Colloid Interface Sci. 1988, 126, 220-230.

[53] Lin, T.-H.; Phillies, G. D. J. J. Colloid Interface Sci. 1984, 100, 82-95.

[54] Utracki, L.; Simha, R. J. Rheology 1981, 25, 329-350.

[55] Takahashi, Y.; Noda, I.; Nagasawa, M. Macromolecules 1985, 18, 2220-2225.

[56] Russo, P. Private Communication, 2004.

[57] Enomoto, H.; Einaga, Y.; Teramoto, A. Macromolecules 1985, 18, 2695-2702.

[58] Phillies, G. D. J.; Peczak, P. Macromolecules 1988, 21, 214-220.

[59] O'Connell, R. O.; Hanson, H.; Phillies, G. D. J. J. Polymer Science Part B Polymer Physics 2004, in press.

[60] Nystrom, B.; Roots, J.; Carlsson, A.; Lindman, B. Polymer 1992, 3 3, 2875.

[61] Nystrom, B.; Walderhaug, H.; Hansen, F. K. J. Phys. Chem. 1993, 97, 7 743.

[62] Brown, W.; Rymden, R. Macromolecules 1986, 19, 2942-2952 .

[63] Langevin, D.; Rondelez, F. Polymer 1978, 19, 875-882.

[64] Phillies, G. D. J. Macromolecules 1998, 31, 2317-2327.

[65] Kivelson, S. A.; Zhao, X.; Kivelson, D.; Fischer, T. M.; Knobler, C. A. J. Chem. Phys. 1994, 101, 2391-2397.

[66] Streletzky, K. A.; Phillies, G. D. J. in *Scattering from Polymers*, ed. Hsiao, B. S. American Chemical Society Symposium Series 2000, 739, 297-316.

[67] For a systematic review of slow mode appearances, see Phillies, G. D. J. Phys. Rev. E 2004, 69, 011801-1-011801-9. For viscosity transitions and their absences in polymer solutions, Phillies, G. D. J., J. Phys. Chem. 1992, 96, 10061-10066.

[68] Streletzky, K. A.; Phillies, G. D. J., unpublished.

[69] Whitford, P. C.; Phillies, G. D. J., J. Chem. Phys. 2005, 122, 044508 1-10.